UNIVERSITY OF CALIFORNIA, SAN DIEGO

Minimally Invasive Principles and Technology to Measure Dynamic Skeletal Muscle Sarcomere Length

A dissertation submitted in partial satisfaction of the
requirements for the degree of Doctor of Philosophy

in

Bioengineering

by

Kevin William Young

Committee in charge:

Professor Richard Lieber, Chair
Professor Geert Schmid-Schonbein, Co-Chair
Professor Joseph Ford
Professor Andrew McCulloch
Professor Stojan Radic
Professor Shankar Subramaniam

2016

The Dissertation of Kevin William Young is approved, and it is acceptable in quality and form for publication on microfilm and electronically:

_____

_____

_____

_____

_____

Co-Chair

_____

Chair

University of California, San Diego

2016

DEDICATION

To my Mom and Dad,

You gave me a world of opportunity and managed to attend all of my sporting events!

Thank you. I love you.

EPIGRAPH

"Two roads diverged in a wood, and I—I took the one less traveled by,
And that has made all the difference."
~Robert Frost

TABLE OF CONTENTS

LIST OF ABBREVIATIONS

LD	Laser diffraction
PGLD	Polarization gated laser diffraction
BF	Bright field
RRS	Resonant reflection spectroscopy
OFDI	Optical frequency domain interferometry
FDTD	Finite difference time domain
RCWA	Rigorous coupled wave analysis
TA	Tibialis anterior
EDL	Extensor digitorum longus
MZM	Mach Zehnder modulator
HNLF	Highly nonlinear fiber
WDM	Wavelength division multiplexer
OSA	Optical spectrum analyzer
FOPO	Fiber optic parametric oscillator
FOPA	Fiber optic parametric amplification
EDFA	Erbium doped fiber amplifier
NIR	Near infrared
SWIR	Short wave infrared

LIST OF FIGURES

LIST OF TABLES

ACKNOWLEDGMENTS

I chose a quote from poet Robert Frost for the epigraph not because I was intent on creating my own path, but because my travel through life and career was far from direct. Along this winding road, however, I've had help, support, and direction from a collection of amazing people. *And that has made all the difference.*

Dr. Lieber, thank you for being my advisor. I've learned tremendously from your analytical mind, but mostly I thank you for your excitement for data and science. I joined this project knowing that it would be challenging, and your enthusiasm helped to keep me going.

Dr. Radic, thank you for being my technical advisor. I am blessed to have been trained in the Photonic Systems Laboratory. The rigor and innovation that I've witnessed is truly amazing.

To my thesis committee, Professors Geert Schmid-Schonbein, Shankar Subramaniam, Joseph Ford, and Andrew McCulloch, thank you for your ideas and support throughout my PhD. To the past and current Muscle Physiology laboratory and collaborators: Sam Ward, Sameer Shah, Simon Shenk, Lori Tuttle, Mary Esparza, Blair Conner, Margie Mathewson, Sudarshan Dayanidhi, Rajeswari Pichika, Tim Tirrell, Rachel Meza, Eugene Sato, Mark Chapman, Ana Rodriguez-Soto, Shawn O'Connor, David Berry, Mike Gibbons, and Shannon Bremmer, thank you for your teaching, help, and kindness. To the past and current members of the Photonic Systems Laboratory: Nikola Alic, Andreas Wiberg, Evgeny Myslivets, Bill Kuo, Vahid Ataie, Ana Pejkic,

Chris Huynh, Daniel Esman, Eduardo Temprana Giraldo, Jin Zhang, Motohiko Eto, Huan Hu, Faezeh Gholami, Ron Nissim, and Lan Liu, thank you for your collaboration, problem solving, and dedication to science. As can be seen from this extensive list, I've been fortunate to work with and exchange ideas with a large number of people. I'd like to further acknowledge Bill Kuo and Shawn O'Connor for their major help with this thesis. Bill, your ability to explain the complex and creatively solve problems is something to aspire to. Shawn, thank you for talking me through the many simple and complex problems we faced in this project.

I would also like to thank my family for being a constant source of support. Mom, Dad, Lauren, Paul, Braden and Emma, I'm thankful for the life and community we are building in San Diego. I treasure our family events.

Finally, thank you Kelsey, my soul mate and best friend. Thank you for the normal days at home. Thank you for our amazing adventures. You make me so happy, I love you.

Chapter 2 is nearly identical to a peer-reviewed article entitled "Polarization gating enables sarcomere length measurements by laser diffraction in fibrotic muscle" by Young KW, Dayanidhi S, and Lieber RL. The article was published in the *Journal of Biomedical Optics* 2014; 19(11):117009-1:4.

Chapter 3 is, in part, nearly identical to sections of a peer reviewed article entitled "Resonant reflection spectroscopy of biomolecular arrays in muscle" by Young KW, Radic S, Myslivets E, O'Connor SM, and Lieber RL. The article was published in *Biophysical Journal* 2014, 107(10):2352-2360.

Chapter 4 is nearly identical to sections of a peer reviewed article entitled "Resonant reflection spectroscopy of biomolecular arrays in muscle" by Young KW, Radic S, Myslivets E, O'Connor SM, and Lieber RL. The article was published in *Biophysical Journal* 2014, 107(10):2352-2360.

Chapter 5 is a combination of sections from two papers. Several sections are nearly identical to sections of a peer reviewed article entitled "Resonant reflection spectroscopy of biomolecular arrays in muscle" by Young KW, Radic S, Myslivets E, O'Connor SM, and Lieber RL. Other sections are nearly identical to a manuscript entitled "In Vivo Minimally-Invasive Molecular Sensing across Millimeters of Muscle Tissue during Movement" by Young KW, Kuo P.-P., O'Connor SM, Radic S, and Lieber RL, that is in preparation for submission to a peer reviewed article.

Chapter 6 is nearly identical to a manuscript entitled "Swept-Pump Fiber Optical Parametric Oscillator with 422 nm Bandwidth and 14 kHz Scan Rate Achieved with Variable Control" by Young KW, Kuo P.-P., Lieber RL, and Radic S, that is in preparation for submission to a peer reviewed article.

This work was funded by the Department of Veteran's Affairs Grant A9028R, NIH Grant R24 HD050837, and private donation by the Elden Foundation.

VITA

2005 – 2009	University of California, Santa Barbara
	Bachelor of Science, Physics
	Minor, Exercise and Health Science
2010 – 2016	University of California, San Diego
	Doctor of Philosophy, Bioengineering

PUBLICATIONS

Journal Articles

Young KW, Kuo BP-P, O'Connor SM, Radic S, and Lieber RL: **In Vivo Minimally-Invasive Protein Sensing across Millimeters of Muscle Tissue During Movement.** (In preparation)

Young KW, Kuo BP-P, Lieber RL, and Radic S: **Swept-Pump Fiber Optical Parametric Oscillator with 422 nm Bandiwdth and 14 kHz Scan Rate.** (In preparation)

O'Connor SM, Cheng EJ, Young KW, Ward SR, Lieber RL: **Sarcomere length distribution quantification in whole muscle frozen sections**. *J Exp Bio*l 2016 (Accepted for publication)

Young KW, Radic S, Myslivets E, O'Connor SM, Lieber RL: **Resonant reflection spectroscopy of biomolecular arrays in muscle**. *Biophys J* 2014, **107**:2352–2360.

Young KW, Dayanidhi S, Lieber RL: **Polarization gating enables sarcomere length measurements by laser diffraction in fibrotic muscle**. *J Biomed Opt* 2014, **19**:117009.

O'Neill PR, Young K, Schiffels D, Fygenson DK: **Few-atom fluorescent silver clusters assemble at programmed sites on DNA nanotubes**. *Nano Lett* 2012, 12:5464–9.

Selected Abstracts

Young KW, Radic S, Myslivets E, O'Connor SM, Lieber RL: **Physiology-first development for resonant reflection spectroscopy of skeletal muscle sarcomeres.** *International Congress on Biophotonics*. Florence (2015).

Young KW, Radic S, Myslivets E, O'Connor SM, Lieber RL: **Sarcomere length measured by novel resonant reflection spectroscopy through fiber optic probes.** *American College of Sports Medicine*. San Diego *(*2014*).*

ABSTRACT OF THE DISSERTATION

Minimally Invasive Principles and Technology to Measure Dynamic Skeletal Muscle Sarcomere Length

by

Kevin William Young

Doctor of Philosophy in Bioengineering

University of California, San Diego, 2016

Professor Richard Lieber, Chair

Professor Geert Schmid-Schonbein, Co-Chair

Skeletal muscle force production results from interaction between actin and myosin protein filaments in repeating units called sarcomeres. Sarcomere force is

transmitted through the basement membrane via protein complexes to a network of connective tissue. Connective tissues transmit force to bone. Typically, muscles are characterized in vitro but this may be insufficient because stresses produced in isolated fibers or muscle bundles differ from whole muscle dynamics. Furthermore, comparisons between normal and diseased muscle states are impossible to make without a proper normalization factor such as sarcomere length. These limitations point to the need for obtaining data in vivo during dynamic movement in the intact muscle. Several tools are available to collect in vivo sarcomere length data, but all fall short of the necessary technical requirements for sarcomere dynamics. To address this need, this dissertation leverages optical communication technology to create new principles and tools to analyze skeletal muscle protein structure.

First, this dissertation improves the sensitivity of existing laser diffraction to measure sarcomere length in fibrotic muscle. Due to an increase in connective tissue, fibrotic muscle scatters laser light and buries the needed diffraction pattern that is used to calculate sarcomere length. Polarization gating is used to filter between scattered and diffracted light to recover the signal and enable sarcomere length measurements.

Second, this dissertation introduces a fundamentally new method to measure sarcomere structure termed resonant reflection spectroscopy (RRS). RRS addresses the challenge of in vivo sarcomere length data collection by illuminating sarcomeres and collecting signals through a single minimally invasive fiber optic probe. Relationships between signal and sarcomere structure are discussed theoretically and simulated in custom made computer code.

Third, proof of concept is demonstrated for RRS measurements of sarcomere

length. A new system, based upon optical communication technology, is built and used to measure sarcomere length in an ensemble of muscles. Validation is demonstrated by comparing sarcomere lengths measured by RRS and traditional laser diffraction. Very high agreement between the methods was achieved.

Fourth, proof of feasibility is demonstrated for minimally-invasive profiling of sarcomere length in muscle during activity and movement. The proof of feasibility system combined RRS with optical frequency domain interferometry (OFDI) to enable profiling sarcomere lengths across millimeters of tissue. Sarcomere lengths are measured with nanometer resolution during passive strain, twitch and tetanic contractions.

Lastly, RRS requires bandwidths and speeds that are inaccessible from commercial laser emitters, and so design rules are developed for swept-pump fiber optic parametric oscillator (FOPO) systems. A FOPO system is demonstrated with 422 nm bandwidth and 14 kHz sweep speed.

Taken together, these demonstrations establish a fundamentally new ability to study movement disorders, including patients with cerebral palsy, stroke, Parkinson's disease and muscular dystrophy.

Chapter 1 Introduction

1.1 General Introduction to the Dissertation

The inability to quantify protein structure and activity *in vivo* is a long standing challenge to understanding tissue, cell, and protein function in human disease. Techniques based on infrared optics are being developed to address this need in multiple organs, but existing techniques fail to achieve adequate resolution and sample rate without significantly damaging tissue. Lack of successful treatment options for patients with muscle dystrophy, Parkinson's disease, stroke, or cerebral palsy are prime examples of the need for such revolutionary technology. The central challenge is caused by the vast scale differences between cellular structures and whole organ function. For example, micrometer length changes to proteins within muscle cells dictate whole muscle force production [1, 2], which corresponds to *five orders of magnitude* change in scale.

Work in this thesis focuses on developing technology to address the challenges mentioned above in skeletal muscle, the largest organ of the body. More specifically, this thesis aims to adapt optical communication theory and technology to minimally invasively measure skeletal muscle sarcomere length. This chapter introduces skeletal muscle microstructure and current, yet inadequate, techniques to measure sarcomere length *in vivo*.

Chapter 2, which has been published in *Journal of Biomedical Optics*, of this dissertation demonstrates using polarization gating to enable sarcomere length measurements by laser diffraction in fibrotic muscle. Laser diffraction (LD)–based measurements of sarcomere length are time-efficient and sample a greater number of

sarcomeres compared with traditional microscopy–based techniques. However, a limitation to LD techniques is that signal quality is severely degraded by scattering events as photons propagate through tissue. Consequently, sarcomere length measurements are unattainable when the number of scattering events is sufficiently large in muscle tissue with a high scattering probability. This occurs in fibrotic skeletal muscle seen in muscular dystrophies and secondary to tissue trauma, thus eliminating the use of LD to study these skeletal muscle ailments. Here, we utilize polarization gating to extract diffracted signals that are buried in noise created by scattering. Importantly, we demonstrate that polarization-gated laser diffraction (PGLD) enables sarcomere length measurements in muscles from chronically immobilized mice hind limbs; these muscles have a substantial increase of intramuscular connective tissue that scatter light and disable sarcomere length measurements by traditional LD. Further, we compare PGLD sarcomere lengths to those measured by bright field (BF) and confocal microscopy as positive controls and reveal a significant bias of BF but not of confocal microscopy.

Chapters 3 and 4, which together have been published in *Biophysical Journal*, demonstrate the first steps to addressing the central problem of measuring sarcomere length with nanometer resolution across millimeters of muscle. Chapter 3 develops theory and Chapter 4 demonstrates feasibility of a new technique, termed resonant reflection spectroscopy (RRS) that measures sarcomere length with submicrometer resolution. In this novel approach, sarcomere structure is measured by the multiple resonant reflections that are uniquely defined by Fourier decomposition of the sarcomere protein spatial framework.

Chapter 5, which is in preparation for submission, provides proof of feasibility for RRS, *in vivo*. We describe a new minimally invasive optical approach that uses a 250 μm fiber optic probe and can acquire data at kHz rates with nm length resolution across mm distances during movement and activity. Our method uses a combination of RRS, which determines tissue microstructure, and optical frequency domain interferometry (OFDI), which controls and measures the precise depth at which the signal is obtained. For the first time, we show analysis of the optical reflections from muscle tissue that easily captures sub-micron sub-millisecond movement of muscle proteins.

Chapter 6, which is in preparation for submission, continues technical development of RRS. Advances in biomedical spectroscopy are driving the need for broadband optical sources. In vivo imaging of biological structures, such as muscle proteins, additionally requires kHz acquisition rates to achieve physiologically relevant data. To address the two key technological requirements of wide bandwidth and fast acquisition, we targeted swept-pump fiber optical parametric oscillator systems. We investigated design rules to maximize bandwidth at kHz sweep rates. We report a new swept-pump fiber optical parametric oscillator with 422 nm total bandwidth and 14 kHz sweep rate.

Chapter 7 summarizes this thesis and discusses the potential impact and future directions of this work.

1.2 Skeletal Muscle Micro-Structure

Interactions between actin and myosin proteins are responsible for many types of cell motility. In striated muscle, actin- and myosin-containing filaments form a hexagonal lattice within each muscle sarcomere [3], the functional unit that creates muscular force. Sarcomeres, in turn, are arranged in series and in parallel within muscle cells [1, 2]. The sliding filament theory [4, 5] explains the geometric relationship between sarcomere length and muscle force production as a result of the precise overlap between actin and myosin filaments. A complex network of proteins [6] and connective tissues [7] integrate sarcomere force to produce movement. Maximal force is produced when actin filaments on each side of the half sarcomere fully envelope the active region of myosin proteins (Fig 1.1).

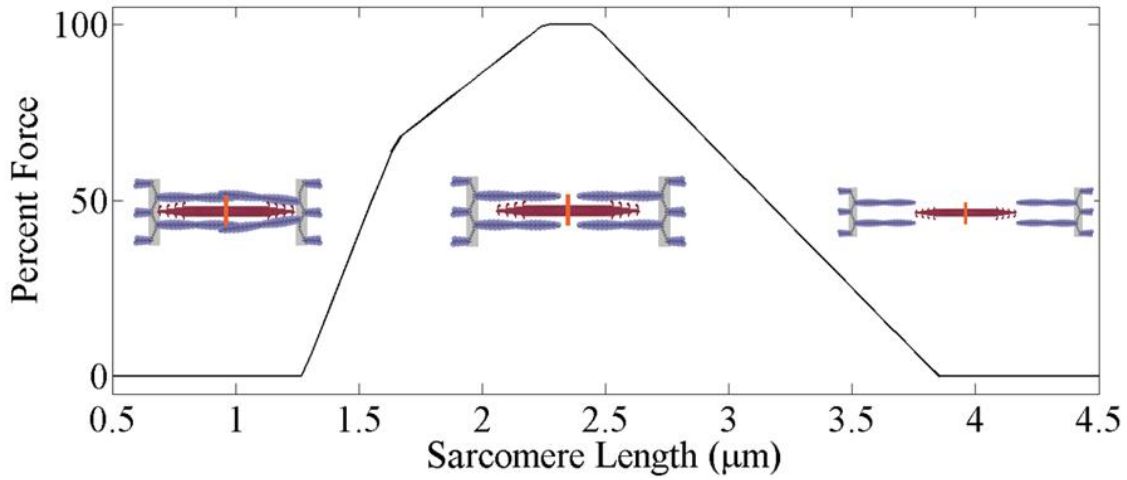

Figure 1.1: Sarcomere force production depends on the overlap and interaction between myosin containing filaments (red) and actin containing filaments (blue). Cartoon sarcomeres depict very short (left), optimal, and very long (right) sarcomere lengths.

Impressively, sarcomere length predicts potential force of muscle fibers [4, 5], even in whole muscles [8]. This relationship between sarcomere length changes and resulting muscular force represents a dramatic change in scale (Fig. 1.2). The five order of magnitude difference between protein structure and tissue physiology is indicative of a central challenge in collecting sufficient data, particularly *in vivo*. Data collection and sampling is discussed further in subsequent sections.

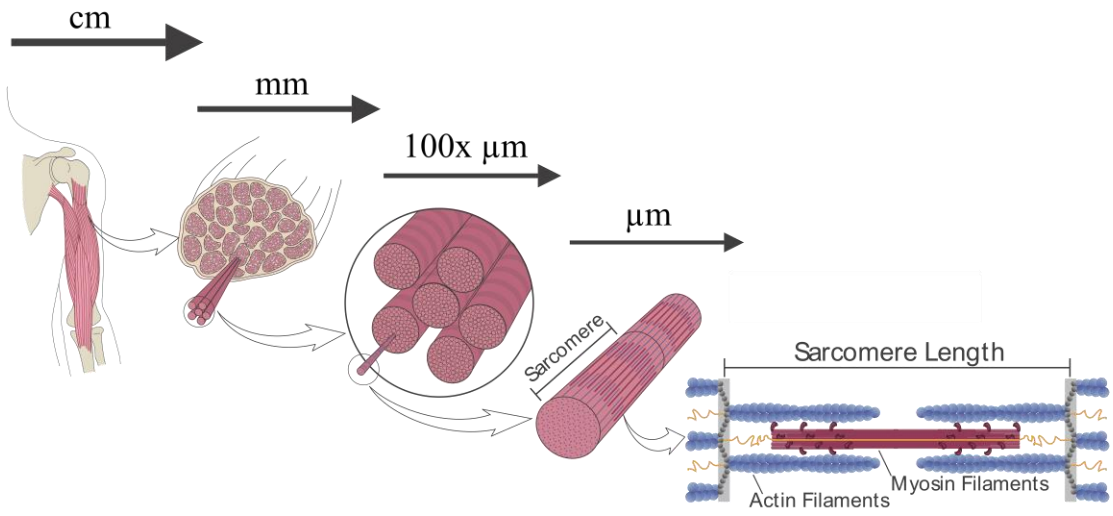

Figure 1.2: Whole muscle force produced in cm scale tissue is dictated by µm scale sarcomeres. Adapted from [9].

There are several lines of evidence that emphasize the importance of sarcomere structure to muscle function. First, the stereotypical sarcomere length range observed during normal human movement provides support for the fact that this length is designed to provide specialized muscle function [10]. Skeletal muscle force production is length-

and velocity dependent [4, 11], and so the relative arrangement of sarcomeres within muscle has a profound impact on function [12]. Additional sarcomeres arranged in series contribute to the ability to produce force during larger excursions, while increased sarcomeres in parallel contribute to higher muscle peak force (Fig 1.3). Second, sarcomere length adaptations after injury provide insights into the mechanism and complexity of the healing process [13]. Third, sarcomeres are abnormally long in hamstring contractures in children with spastic cerebral palsy [14], which fundamentally limits the muscle's ability to produce force and demonstrates the complex interaction between the muscular and nervous systems. Furthermore, altered sarcomere filament dimensions are implicated in causing muscular disease [15, 16].

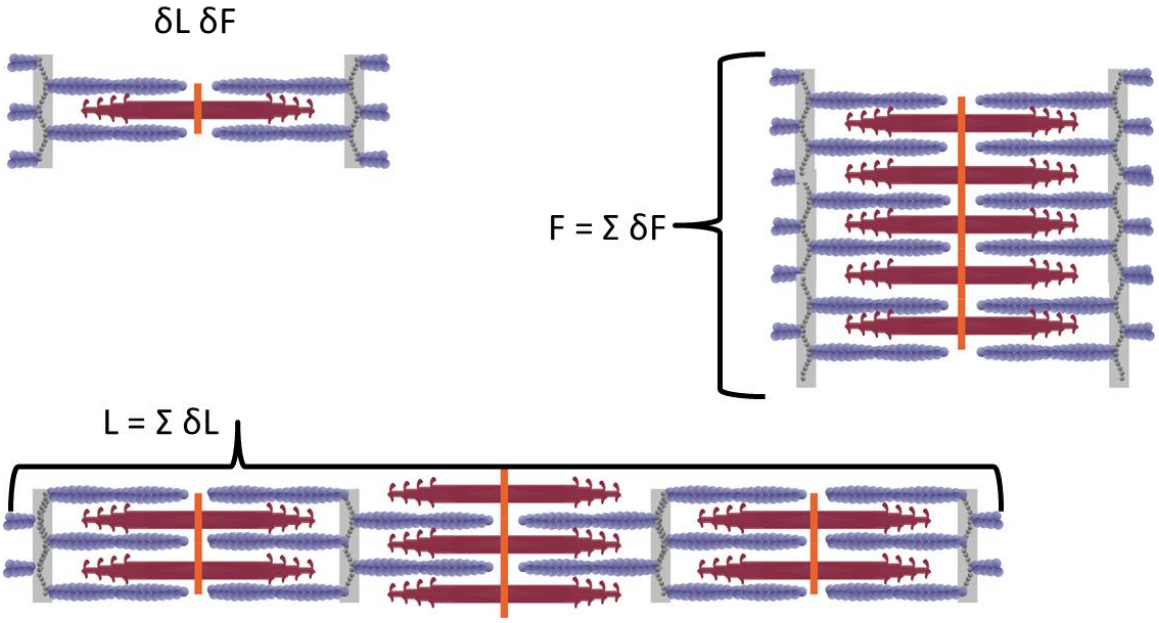

Figure 1.3: Cartoons exhibit conceptual addition of sarcomere force and excursion. Sarcomeres in series add to total muscle excursion. Sarcomeres in parallel add to total muscle force.

1.3 State of the Art Tools to Measure Muscle Sarcomere Length

Several tools are available to collect *in vivo* sarcomere length data, but all fall short of the necessary technical requirements for sarcomere dynamics; simultaneous sampling across millimeters of muscle tissue, sampling at kilohertz rates, compatibility with gross movement, inducing minimal tissue damage, and achieving nanometer length resolution. Intraoperative laser diffraction provided the first direct, *in vivo* sarcomere length measurement in humans during hand surgery [17, 18]. Originating from work in the 1970s [1], laser diffraction (LD) based methods are widely used to measure sarcomere length. Trans-illumination of muscle fibers by laser light yields a diffraction pattern, and the grating equation [9] relates diffraction pattern periodicity to the periodicity of the muscle striation pattern and, therefore, sarcomere length (Fig. 1.4).

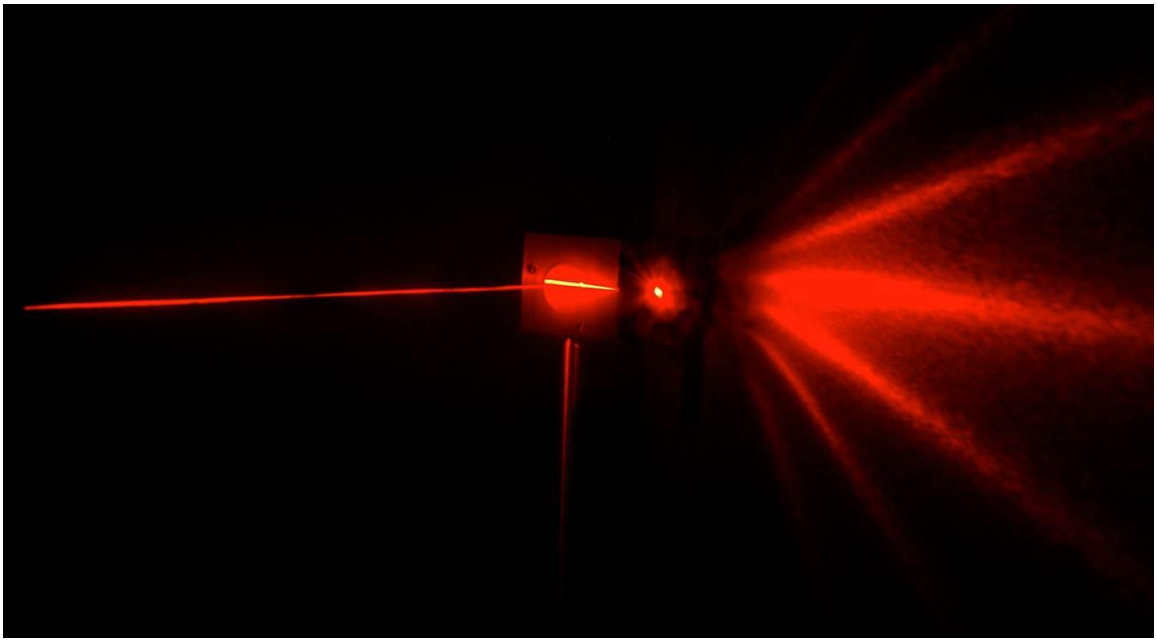

Figure 1.4: Laser illumination of skeletal muscle results in a diffraction pattern. Separation between diffracted beams is used to calculate sarcomere length. Adapted from [21].

LD based methods have been used to measure and understand the role of sarcomere length in a variety of physiological studies, including: abnormally-long resting sarcomere lengths in muscular deformities in children with spastic cerebral palsy [10], intraoperative sarcomere lengths before and after surgical tendon lengthening [11], and in muscle architecture studies of the lumbar spine [12]. The major utility of LD is the fact that it rapidly samples hundreds of thousands of sarcomeres that are illuminated by the beam. However, this tool is only suitable for passive measurement of sarcomere length during surgical procedures and is not incompatible with dynamic motion.

An emerging, less invasive method for measuring *in vivo* sarcomere length is microendoscopy [22]. Recently, microendoscopy was used in conjunction with electrical stimulation in a case study of human sarcomere lengths [23]. This report shows interesting passive data, but appears limited to long sarcomeres at significant passive tension. While muscle twitches were reported, microendoscopy is a point scanning technique that imposes a necessary trade-off between sample size and sample rate. This limitation restricts the data to only a few sarcomeres. Unfortunately, we found that sampling less than thousands of sarcomeres leads to sampling bias [20]. This applies to all microscopy-based methods, which are limited to the system's field of view and depth of field, which typically includes only hundreds of sarcomeres [13], non-planar optical artifacts, and the need for significant tissue pre-processing.

Additionally, microendoscopy measured sarcomere displacement rather than sarcomere shortening, which permits misinterpretations based on relative motion of the probe and between sarcomere lengthening or shortening. Microendoscopy also requires

tightly focused beams from a lensed system and is unlikely to have needle size smaller than the achieved 0.9 mm diameter. Smaller needles are more compatible with gross movement and less likely to cause pain [24].

Due to these considerations, we pursue only diffraction based rather than microscopy based methods to measure sarcomere length. The next chapter introduces using polarization gating to enable sarcomere length measurements by laser diffraction in fibrotic muscle tissue. Scattering is a large cause of noise in diffraction based methods, so understanding scattering behavior and being able to minimize its effect is critical for new technology development.

1.5 References

1. Huxley AF, Niedergerke R: **Structural Changes in Muscle During Contraction: Interference Microscopy of Living Muscle Fibres**. *Nature* 1954, **173**:971–973.

2. Huxley H, Hanson J: **Changes in the Cross-Striations of Muscle during Contraction and Stretch and their Structural Interpretation**. *Nature* 1954, **173**:973–976.

3. Millman BM: **The filament lattice of striated muscle.** *Physiol Rev* 1998, **78**:359–91.

4. Gordon A, Huxley A, Julian F: **The variation in isometric tension with sarcomere length in vertebrate muscle fibres**. *J Physiol* 1966, **184**:170–192.

5. Gordon A, Huxley A, Julian F: **Tension development in highly stretched vertebrate muscle fibres**. *J Physiol* 1966, **184**:143–169.

6. Lazarides E: **Intermediate filaments as mechanical integrators of cellular space**. *Nature* 1980, **283**:249–256.

7. Gillies AR, Lieber RL: **Structure and function of the skeletal muscle extracellular matrix.** *Muscle Nerve* 2011, **44**:318–31.

8. Winters T, Takahashi M, Lieber R, Ward S: **Whole muscle length-tension relationships are accurately modeled as scaled sarcomeres in rabbit hindlimb muscles**. *J Biomech* 2011, **44**:109–115.

9. Mathewson MA, Lieber RL: **Pathophysiology of Muscle Contractures in Cerebral Palsy**. *Phys Med Rehabil Clin North Am* 2015, **26**:57–67.

10. Burkholder TJ, Lieber RL: **Sarcomere length operating range of vertebrate muscles during movement**. *J Exp Biol* 2001, **204**(Pt 9):1529–1536.

11. Hill a. V.: **The Mechanics of Active Muscle**. *Proc R Soc B Biol Sci* 1953, **141**:104–117.

12. Lieber RL, Ward SR: **Skeletal muscle design to meet functional demands.** *Philos Trans R Soc Lond B Biol Sci* 2011, **366**:1466–76.

13. Williams PE, Goldspink G: **The effect of immobilization on the longitudinal growth of striated muscle fibres.** *J Anat* 1973, **116**(Pt 1):45–55.

14. Smith LR, Lee KS, Ward SR, Chambers HG, Lieber RL: **Hamstring contractures in children with spastic cerebral palsy result from a stiffer extracellular matrix and increased in vivo sarcomere length.** *J Physiol* 2011, **589**(Pt 10):2625–39.

15. Bang M-L, Li X, Littlefield R, Bremner S, Thor A, Knowlton KU, Lieber RL, Chen J: **Nebulin-deficient mice exhibit shorter thin filament lengths and reduced**

contractile function in skeletal muscle. *J Cell Biol* 2006, **173**:905–16.

16. Ottenheijm C a C, Witt CC, Stienen GJ, Labeit S, Beggs AH, Granzier H: **Thin filament length dysregulation contributes to muscle weakness in nemaline myopathy patients with nebulin deficiency.** *Hum Mol Genet* 2009, **18**:2359–69.

17. Fleeter TB, Adams JP, Brenner B, Podolsky RJ: **A laser diffraction method for measuring muscle sarcomere length in vivo for application to tendon transfers**. *J Hand Surg Am* 1985, **10**:542–546.

18. Lieber RL, Loren GJ, Fridén J: **In vivo measurement of human wrist extensor muscle sarcomere length changes.** *J Neurophysiol* 1994, **71**:874–81.

19. Cleworth D, Edman K: **Changes in sarcomere length during isometric tension development in frog skeletal muscle**. *J Physiol* 1972, **227**:1–17.

20. Young KW, Dayanidhi S, Lieber RL: **Polarization gating enables sarcomere length measurements by laser diffraction in fibrotic muscle**. *J Biomed Opt* 2014, **19**:117009.

21. Mathewson MA, Ward SR, Chambers HG, Lieber RL: **High resolution muscle measurements provide insights into equinus contractures in patients with cerebral palsy**. *J Orthop Res* 2015, **33**:33–39.

22. Llewellyn ME, Barretto RPJ, Delp SL, Schnitzer MJ: **Minimally invasive high-speed imaging of sarcomere contractile dynamics in mice and humans.** *Nature* 2008, **454**:784–8.

23. Sanchez GN, Sinha S, Liske H, Chen X, Nguyen V, Delp SL, Schnitzer MJ, Sanchez GN, Sinha S, Liske H, Chen X, Nguyen V, Delp SL: **Case Study In Vivo Imaging of Human Sarcomere Twitch Dynamics in Individual Motor Units Case Study In Vivo Imaging of Human Sarcomere Twitch Dynamics in Individual Motor Units**. *Neuron* 2015, **88**:1109–1120.

24. Gill HS, Prausnitz MR: **Does needle size matter?** *J Diabetes Sci Technol* 2007, **1**:725–9.

Chapter 2 Polarization Gating Enables Sarcomere Length Measurement by Laser Diffraction in Fibrotic Muscle

2.1 Introduction

Muscle and connective tissues are birefringent and heavily scattering media, and, therefore, diffraction signals are degraded by scattering events as light propagates through tissue [14]. At distances exceeding a few mean free paths (average distance between light-tissue interactions), light enters the "diffuse" [15] regime of propagation and diffracted signals cannot be detected. The reduced scattering coefficient is larger with increased connective tissue associated with many muscle pathologies [16, 17], and increased scattering typically makes it impossible to measure diffraction patterns from fibrotic tissues. Some clinical and experimental examples that show connective tissue increases in muscle include: muscular dystrophies [18], developmental disorders such as cerebral palsy [10], immobilization [19] and aging [20].

Detailed models of diffraction [21] and diffuse propagation of polarized light [14, 22] suggest that they differently alter polarization state. So, the signal exiting a highly scattering muscle sample is a polarization sensitive superposition of diffracted light and diffuse transmittance. As a result, we tested whether polarization gated laser diffraction (PGLD) could extract diffracted signals from diffuse noise and thus enable sarcomere length measurement.

We built a PGLD system and used it to recover diffracted signals in fibrotic soleus muscles from chronically immobilized murine hind limbs. Importantly, LD was unable to measure sarcomere lengths in these highly scattering muscles. We also

compared sarcomere lengths measured by PGLD to bright field (BF) microscopy and found a significant bias. By using confocal microscopy as an additional positive control, we saw that BF measurements of these fibers, rather than PGLD measurements, suffer from sampling bias.

2.2 Methods

2.2.1 Sarcomere Length Measurement by Polarization Gated Laser Diffraction

To perform sarcomere length measurement by LD, a 633 μm wavelength He-Ne laser trans-illuminated tissue samples (Fig. 2.1). The resultant diffraction pattern and diffuse transmitted light illuminated a measurement screen and spacing between diffracted peaks (if present) was measured by digital calipers and used to solve for sarcomere length using the grating equation [9]:

$$SL = \frac{m\lambda}{\sin(\theta_m)} \quad (1)$$

where SL is sarcomere length, m is diffraction order, λ is laser wavelength, and θ_m is angle to diffraction peak for order *m*. Calibration of the distance between sample and diffraction screen was performed using a standardized 2 μm and 3 μm diffraction gratings.

Polarization gating was performed by inserting linear polarizers in rotary optic mounts (#52-574, Edmund Optics Inc., Barrington, NJ) above and below the sample stage (Fig. 2.1). The linear polarization angle for each polarizer could be adjusted manually with 0.5° accuracy. Polarization angles for both polarizers were manually adjusted to maximize diffraction patterns visually.

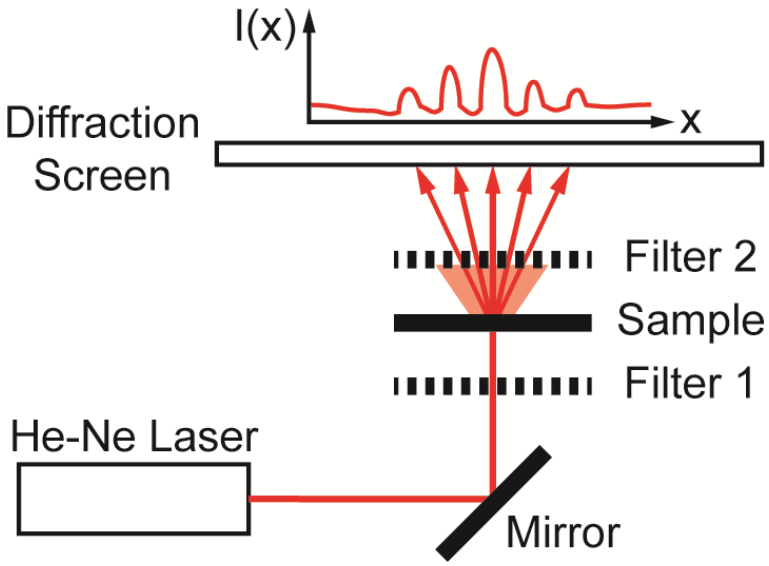

Figure 2.1: Sarcomere length measured by polarization gated laser diffraction (PGLD). Polarizing filters extract diffraction signal from superimposed noise.

Though sarcomere length measurements were made manually, a stationary camera was used to image the diffraction screen as an example of PGLD signal extraction. Images were processed using MATLAB (The MathWorks, Inc., Natick, Massachusetts, United States) to obtain an average signal intensity plotted against the long axis of the muscle fibers.

2.2.2 Hindlimb Immobilization to generate Highly Scattering Muscle

One hindlimb each of four 8 week old wild-type (C57BL/6) mice were immobilized in paris casts for 14 days such that the ankle was in dorsiflexion (42.4°±12.5°) stretching the soleus muscle, following the protocol of Williams and Goldspink [23]. The contralateral uncasted hindlimb served as controls. The casts were

repaired as needed to ensure that the integrity of the casts were maintained throughout 2 weeks.

2.2.3 Tissue Preparation

Hindlimbs from the euthanized immobilized mice were disarticulated at the hip, skinned, pinned to a cork board at a fixed angle of 90° at the knee and ankle and chemically fixed in 10% Formalin for two days. Whole tibialis anterior (TA) and soleus muscles were surgically removed then rinsed and stored in 1X Phosphate buffered saline. To facilitate fiber bundle dissection, muscles were partially digested in 15% H_2SO_4 for 30 minutes, similar to the protocol of Shah et al. 2001 [24]. Fiber bundles containing 1-10 myofibers were microdissected under a microscope, and mounted on a glass slide for sarcomere length measurements. 10-15 fiber bundles were dissected from each muscle.

2.2.4 Light Microscopy

A microscope (Model DM6000, Leica Microsystems Inc., Buffalo Grove, Illinois) was used to take BF images of soleus and TA muscle fiber bundles using a 40X objective. ImageJ software [25] was used to average 10-30 sarcomere lengths in series within an image. Measured regions were chosen based on ability to clearly see the sarcomeres-in-series, unimpaired by the increased connective tissue.

Confocal bright field microscopy (Model SP5, Leica Microsystems Inc., Buffalo Grove, Illinois) was used to sample sarcomere length through a muscle fiber bundle with a 63X objective. Focal depth was adjusted to image at least 50 focal planes through each fiber bundle (0.5-1.5 µm Sol, 2.5-3.5 µm TA). In each focal plane, sarcomere length was

averaged across 10 in-focus sarcomeres in series. Measured regions of muscle fiber bundles were marked on the slide, and the same volume of muscle was measured by PGLD.

2.2.5 Data Analysis

Statistical tests were made using Prism (GraphPad Software, Inc., La Jolla, California, United States) using a significance level (α) of 0.05. Average sarcomere length measured by PGLD and BF were compared in 4 immobilized soleus muscles in a two-way ANOVA with main effects of measurement technique and muscle sample. We did not use a paired t-test because the exact sampled location was not the same between tests. However, we did measure the same volume of muscle with PGLD and confocal microscopy and used a paired t-test and intraclass correlation equation 2-1.

2.3 Results and Discussion

2.3.1 Polarization Gating Rescue Diffracted Signals

Sarcomere lengths from murine soleus muscles harvested from hindlimbs treated with prolonged immobilization could not be measured by traditional LD, due to increased connective tissue content that erodes the diffracted signal with scattering events and buries the signal in diffuse transmitted light and laser speckle (Fig. 2.2). However, the diffraction pattern was readily visualized using PGLD, which enabled comparison between sarcomere lengths in fibrotic muscles without sampling bias.

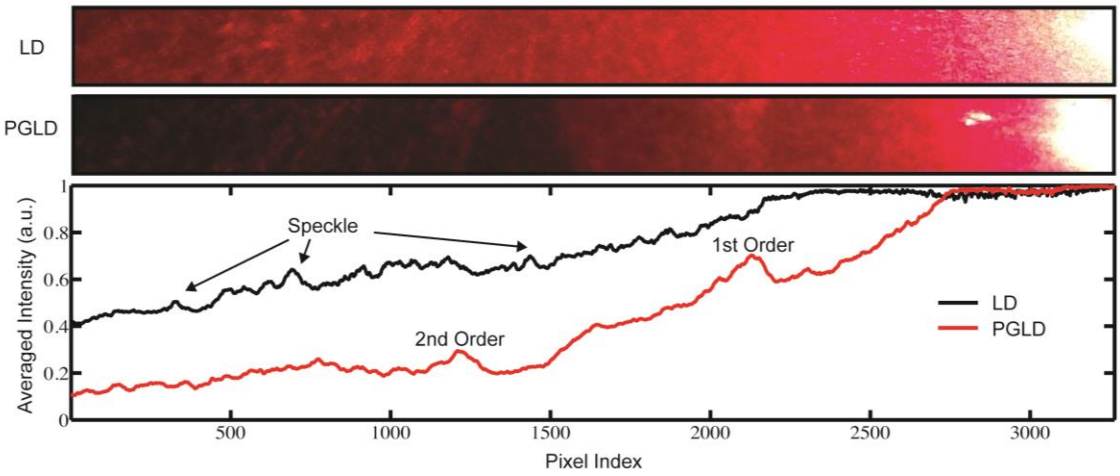

Figure 2.2: Polarization gated laser diffraction (PGLD) extracts diffraction patterns from superimposed diffuse noise.

For our proof-of-principle study we used simple linear polarizing filters for two reasons: they are simple to use and Li et al. [26] showed that diffuse propagation of circular polarization and linear polarization are similar in muscle. However, it is possible that the signal-to-noise ratio and sensitivity can be further improved by exploring all polarization combinations.

2.3.2 Sarcomere Lengths measured by PGLD and Bright Field Microscopy

We compared sarcomere lengths from muscle fiber bundles of 4 immobilized soleus muscles measured by PGLD and BF (Fig. 2.3). Sarcomere length measured in a normal TA muscle with traditional LD was included for reference. Note that polarization gating does not shift the location of diffracted peaks. Statistical analysis by two-way ANOVA shows a significant effect of measurement technique ($p < 0.001$), a significant effect of muscle sample ($p < 0.001$), and no significant interaction term ($p = 0.385$). These data suggest a systematic bias between sarcomere lengths measured by PGLD and

BF (0.19 µm average difference), which was seen despite the varied sarcomere lengths in each muscle sample. This disagreement was surprising because diffraction and microscopy techniques are considered standard methods to measure sarcomere length. However, BF samples a volume of sarcomeres from the muscle fiber bundle that is in focus, whereas PGLD samples throughout the bundle thickness. So, BF may under sample or have a regional sampling bias that results in the sarcomere length disagreement. As an additional positive control, we thus compared PGLD to confocal microscopy images taken throughout the muscle fiber bundle thickness which we believed would provide a more accurate comparison.

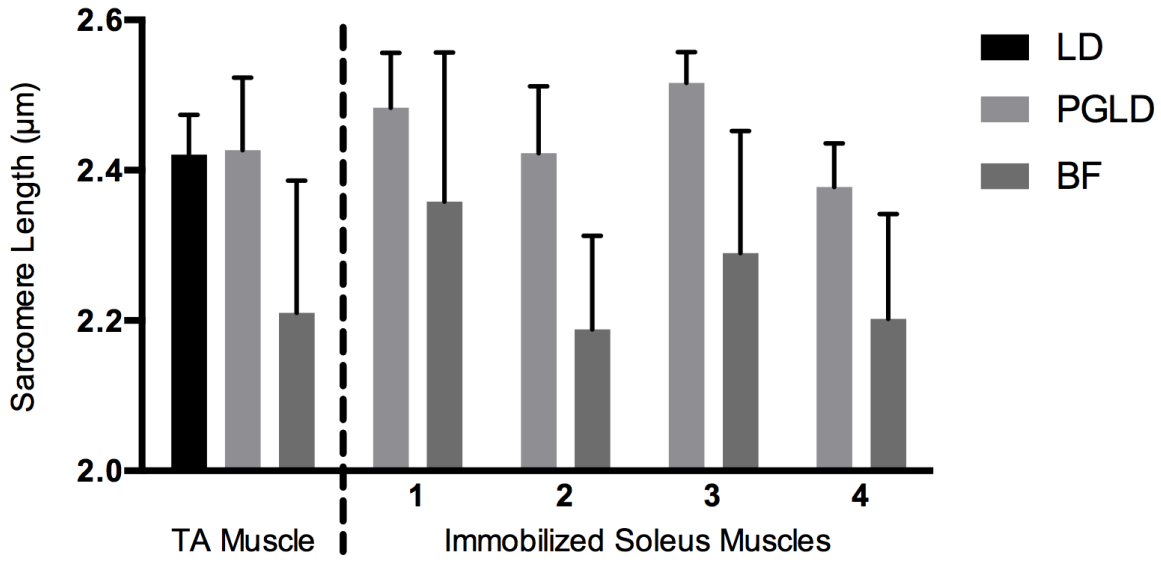

Figure 2.3: Sarcomere Length (mean ± standard deviation, n= 5-15 measurements per muscle) measured by laser diffraction (LD), polarization gated laser diffraction (PGLD), and bright field microscopy (BF). In immobilized muscles, sarcomere length measurement by traditional LD method was not possible. Two-way ANOVA revealed a significant effect of measurement technique ($p < 0.001$), a significant effect of muscle sample ($p < 0.001$), and no significant interaction term ($p > 0.3$).

2.3.3 Sarcomere Lengths Measured by PGLD and Confocal Microscopy

Data presented above suggested a systematic bias leading to different sarcomere length measurements between PGLD and BF. We hypothesized that relatively small numbers of sarcomeres measured by BF at specific depths of focus in the fiber bundles produced this bias. We thus performed a rigorous comparison of sarcomere lengths measured by PGLD and confocal microscopy, because confocal microscopy is able to image throughout the muscle fiber bundle volume (Fig. 2.4).

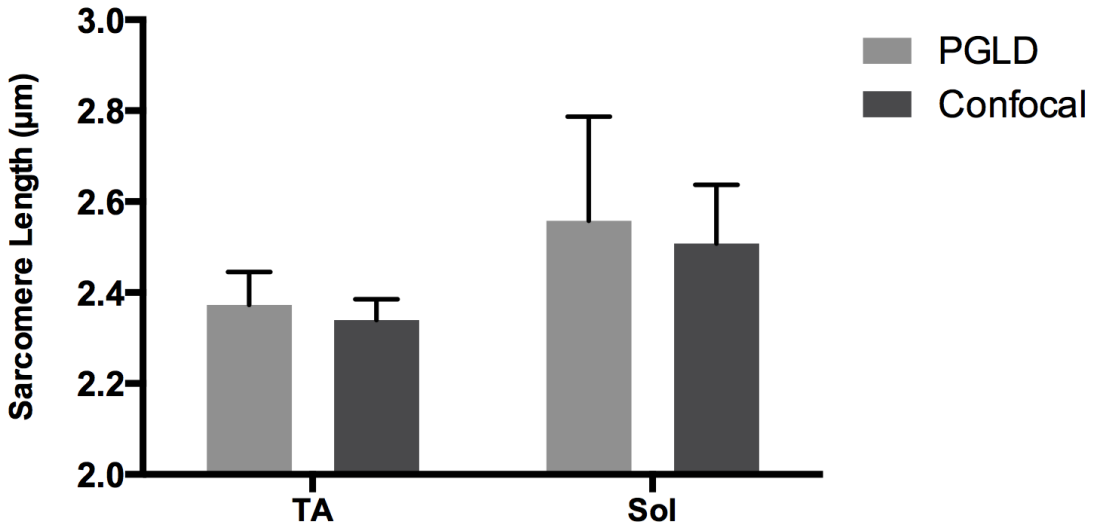

Figure 2.4: PGLD enables sarcomere length measurements in highly scattering muscle tissue. No significant differences were found between the two methods ($p = 0.14$). Data shown are mean ± standard deviation ($n = 10$ muscles).

Paired t-test comparing sarcomere length measured by PGLD and confocal microscopy in 10 fiber bundles (5 from normal TA, 5 from immobilized soleus) showed no significant difference ($p = 0.14$) with 80% power to detect a 0.08 µm difference. This serves as a positive control for the new PGLD sarcomere length method, and highlights the need to obtain appropriate samples to accurately perform such comparisons. We also

assessed the agreement between the two methods with linear and intraclass correlation (Fig 2.5). There was a significant correlation ($p < 0.001$; $r^2 = 0.875$; $ICC_{2,1} = 0.870$)

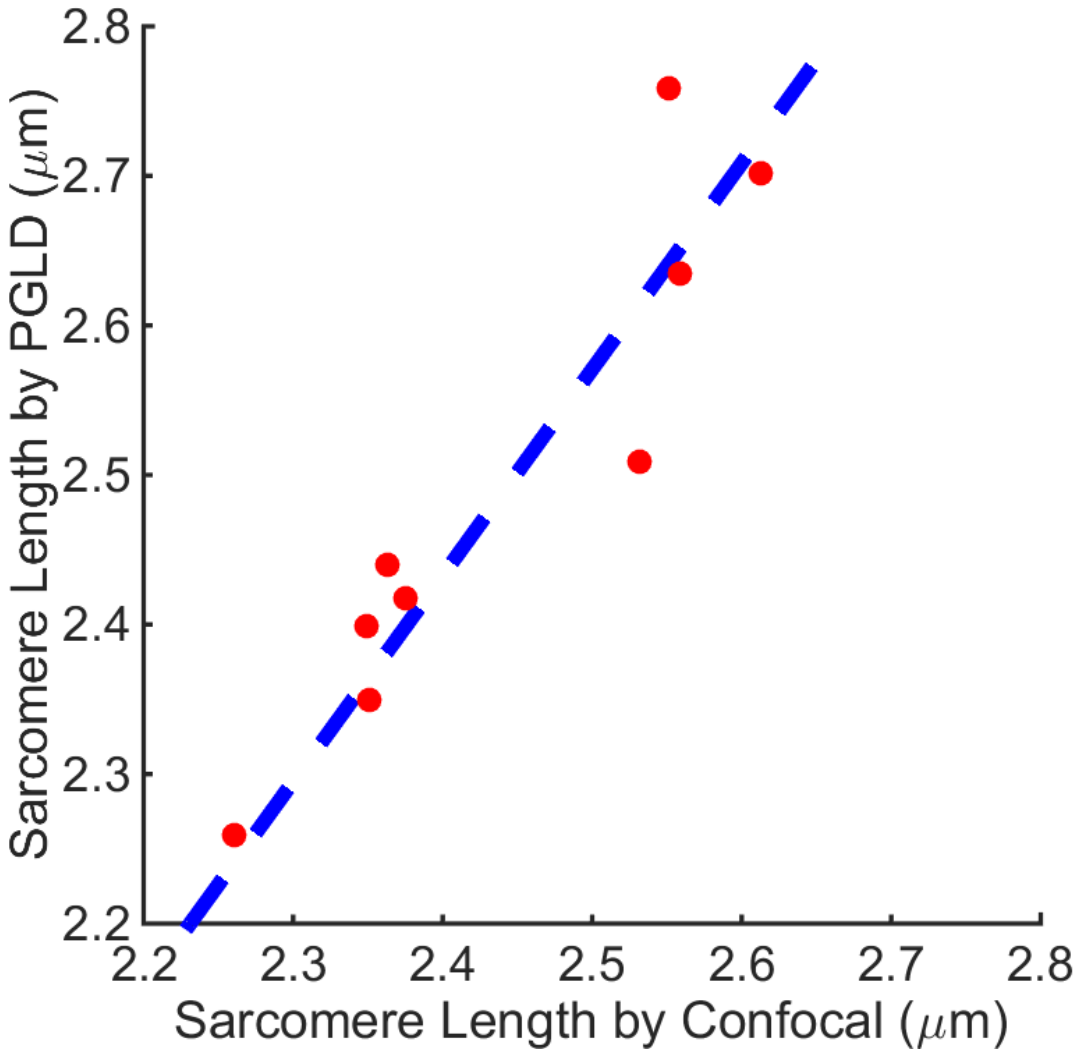

Figure 2.5: Sarcomere lengths measured by confocal microscopy and polarization gated laser diffraction are significantly correlated ($p<0.001$; $r^2 = 0.875$) and have excellet agreement ($ICC_{2,1} = 0.870$)

2.3.4 Trade-offs of Several Sarcomere Length Measurement Methods

There are several important differences among these measurement methods (Table 2.1). LD was only successful in 7 of 115 fiber bundles obtained from immobilized muscles. Using PGLD drastically improved the sensitivity to 92 of 115, a 1333% improvement in measurement ability. We did not perform BF and confocal microscopy on all 115 fiber bundles, but our experience suggests that 100% sensitivity can be achieved with these techniques if enough time is spent. High sensitivity, however, is balanced by measurement time and sampling bias. BF has high sensitivity, but we yielded a significant bias of 0.19 μm shorter sarcomere lengths. Confocal microscopy also has high sensitivity, but it takes significantly longer to perform than PGLD. Sample size was estimated using the following parameters: 1 μm diameter and 2.5 μm length sarcomeres, 1 mm laser beam width, and 50 μm depth of field.

Table 2.1: PGLD enables sarcomere length measurements in highly scattering muscle.

	LD	**PGLD**	**BF**	**Confocal**
Sample Size	Hundreds of Thousands	Hundreds of Thousands	Hundreds	Thousands
Selection Bias	Lowest	Lowest	Highest	Low
Sensitivity in Fibrotic Tissue	7/115	92/115	115/115*	115/115*
Measurement Time	Minutes	Minutes	Minutes to Hours	Hours

*Not attempted in all 115 samples, though samples can be found after sufficient search.

2.4 Conclusion

We demonstrated that polarization gated laser diffraction successfully and accurately recovers diffracted signals in highly scattering muscle tissue which were previously impossible to measure by LD. This method is an example of a simple

technical adjustment that can be used to increase the sensitivity of laser diffraction. Diffraction based methods efficiently sample large numbers of compared to microscopy based techniques.

2.5 Acknowledgements

Chapter 2 is nearly identical to a peer reviewed article entitled “Polarization gating enables sarcomere length measurements by laser diffraction in fibrotic muscle" by Young KW, Dayanidhi S, Lieber RL. The article was published in *Journal of Biomedical Optics* 2014, 19(11):117009-1-117009-5. Research reported in this publication was supported by the National Institute of Child Health and Human Development of the National Institutes of Health under Award Number R24 HD050837; by the National Institute of Arthritis and Musculoskeletal and Skin Diseases of the National Institutes of Health under Award Numbers P30 AR061303 and R01 AR057393; and by the Department of Veteran’s Affairs Grant A9028R. The content is solely the responsibility of the authors and does not necessarily represent the official views of the National Institutes of Health. The authors thank Peter Dykstra for his assistance with the confocal microscope experiments.

2.6 References

1. Cleworth D, Edman K: **Changes in sarcomere length during isometric tension development in frog skeletal muscle**. *J Physiol* 1972, **227**:1–17.

2. Gordon A, Huxley A, Julian F: **The variation in isometric tension with sarcomere length in vertebrate muscle fibres**. *J Physiol* 1966, **184**:170–192.

3. Gordon A, Huxley A, Julian F: **Tension development in highly stretched vertebrate muscle fibres**. *J Physiol* 1966, **184**:143–169.

4. Gans C: **Fiber architecture and muscle function**. *Exerc Sport Sci Rev* 1982, **10**:160–207.

5. Lieber RL, Fridén J: **Functional and clinical significance of skeletal muscle architecture.** *Muscle Nerve* 2000, **23**:1647–66.

6. Powell P, Roy R, Kanim P, Bello M, Edgerton V: **Predictability of skeletal muscle tension from architectural determinations in guinea pig hindlimbs**. *J Appl Physiol* 1984, **57**:1715–1721.

7. Huxley AF, Niedergerke R: **Structural Changes in Muscle During Contraction: Interference Microscopy of Living Muscle Fibres**. *Nature* 1954, **173**:971–973.

8. Huxley H, Hanson J: **Changes in the Cross-Striations of Muscle during Contraction and Stretch and their Structural Interpretation**. *Nature* 1954, **173**:973–976.

9. Lieber RL, Yeh Y, Baskin RJ: **Sarcomere length determination using laser diffraction. Effect of beam and fiber diameter.** *Biophys J* 1984, **45**:1007–16.

10. Smith LR, Lee KS, Ward SR, Chambers HG, Lieber RL: **Hamstring contractures in children with spastic cerebral palsy result from a stiffer extracellular matrix and increased in vivo sarcomere length.** *J Physiol* 2011, **589**(Pt 10):2625–39.

11. Fridén J, Lieber RL: **Physiologic consequences of surgical lengthening of extensor carpi radialis brevis muscle-tendon junction for tennis elbow.** *J Hand Surg Am* 1994, **19**:269–74.

12. Ward SR, Kim CW, Eng CM, Gottschalk LJ, Tomiya A, Garfin SR, Lieber RL: **Architectural analysis and intraoperative measurements demonstrate the unique design of the multifidus muscle for lumbar spine stability.** *J Bone Joint Surg Am* 2009, **91**:176–85.

13. Llewellyn ME, Barretto RPJ, Delp SL, Schnitzer MJ: **Minimally invasive high-speed imaging of sarcomere contractile dynamics in mice and humans.** *Nature* 2008, **454**:784–8.

14. Wang X, Wang L V: **Propagation of polarized light in birefringent turbid media: a Monte Carlo study.** *J Biomed Opt* 2002, **7**:279–90.

15. Bartel S, Hielscher AH: **Monte Carlo simulations of the diffuse backscattering Mueller matrix for highly scattering media**. *Appl Opt* 2000, **39**:1580–1588.

16. Xia JJ, Berg EP, Lee JW, Yao G: **Characterizing beef muscles with optical scattering and absorption coefficients in VIS-NIR region.** *Meat Sci* 2007, **75**:78–83.

17. Lieber RL, Ward SR: **Cellular mechanisms of tissue fibrosis. 4. Structural and functional consequences of skeletal muscle fibrosis.** *Am J Physiol Cell Physiol* 2013, **305**:C241–52.

18. Zhou L, Lu H: **Targeting fibrosis in Duchenne muscular dystrophy.** *J Neuropathol Exp Neurol* 2010, **69**:771–6.

19. Williams PE, Goldspink G: **Connective tissue changes in immobilised muscle**. *J Anat* 1984, **138**:343–350.

20. Mann CJ, Perdiguero E, Kharraz Y, Aguilar S, Pessina P, Serrano AL, Muñoz-Cánoves P: **Aberrant repair and fibrosis development in skeletal muscle.** *Skelet Muscle* 2011, **1**:21.

21. Sidick E, Knoesen a, Xian JK, Yeh Y, Baskin RJ: **Rigorous analysis of light diffraction by a striated muscle fibre.** *Proc Biol Sci* 1992, **249**:247–57.

22. Shuaib A, Li X, Yao G: **Transmission of polarized light in skeletal muscle.** *J Biomed Opt* 2011, **16**:025001.

23. Williams PE, Goldspink G: **Longitudinal growth of striated muscle fibres**. *J Cell Sci* 1971, **9**:751–767.

24. Shah SB, Peters D, Jordan K a, Milner DJ, Fridén J, Capetanaki Y, Lieber RL: **Sarcomere number regulation maintained after immobilization in desmin-null mouse skeletal muscle.** *J Exp Biol* 2001, **204**(Pt 10):1703–10.

25. Rasband WS: **ImageJ**. *U.S. National Institutes of Health, Bethesda, Maryland, USA* .

26. Li X, Ranasinghesagara JC, Yao G: **Polarization-sensitive reflectance imaging in skeletal muscle**. *Opt Express* 2008, **16**:9927.

Chapter 3 Theoretical development of resonant reflection spectroscopy

3.1 Introduction

Many studies highlight the need to study sarcomere structure in normal and abnormal muscle, but they require substantial effort to obtain useful data because available techniques are ex vivo [1] or require highly-invasive surgical settings [2, 3]. These restrictions and challenges have crippled data collection and therefore research progress, especially in humans. In vivo and real time techniques to measure sarcomere length are needed to understand human muscle function, diagnose muscle pathology and assist with surgical and nonsurgical muscle therapies.

Several techniques were developed to address these challenges, but none satisfy all requirements for in vivo research. One emerging method is called minimally invasive optical microendoscopy [4, 5], which is a point-scanning technique that leverages nonlinear optical signal generation in the myosin rod domain. Microendoscopy is likely to find research application, but nonlinear processes in tissue are highly inefficient and require strongly focused beams. Tightly confining light into heterogeneous material, such as tissue, and the significant consequences of motion artifacts in point scanning techniques severely limit the widespread adoption of microendoscopy, especially for functional studies. Even if resolved, intensities required for nonlinear optics use in tissue can cause thermal damage or laser ablation [6], motivating the need for a new, low light intensity method. In response to these needs, we discovered that resonant reflections from sarcomeres are wavelength dependent and can reveal protein structural information

through low power resonant reflection spectroscopy (RRS). In this work, we describe a theoretical model that relates sarcomere structure to expected signal spectra.

RRS is based on the notion that light transmission or reflection in a material with periodically patterned refractive index can be uniquely related to its underlying structure [7–9]. The best-known example of this phenomenon is laser illumination of diffraction gratings, where grating periodicity is synthesized from angular separation between bright regions in the resulting diffraction pattern. More specifically, the diffraction pattern represents the grating structure in the spatial frequency domain [9] through Fourier relationships [10]. Given that muscle protein organization repeats periodically with every sarcomere length along a muscle fiber, and that refractive index is proportional to protein density, light propagation through muscle fibers can be analyzed identically to diffraction gratings with grating period equal to sarcomere length [1, 11].

Laser diffraction (LD) has been used to measure sarcomere length since the 1970s [1], though it has remained largely unchanged despite tremendous progress in optical technology (Fig. 3.1*A*). Using this technique in vivo requires invasive procedures to access the diffraction pattern of the monochromatic signal. To circumvent this limitation, we illuminate muscle fibers co-linearly using broad polychromatic illumination to transform sarcomere structure information into the optical frequency domain. This is accomplished in RRS by measuring intensity of resonant reflections across optical wavelengths (Fig. 3.1*B*), rather than measuring intensity of a spatial diffraction pattern, as in LD. Using the optical frequency domain allows illumination and reflected light to

traverse the same path, enabling the use of the smallest minimally invasive needle probes that have been demonstrated for in vivo optical-signal collection in muscle tissue [12].

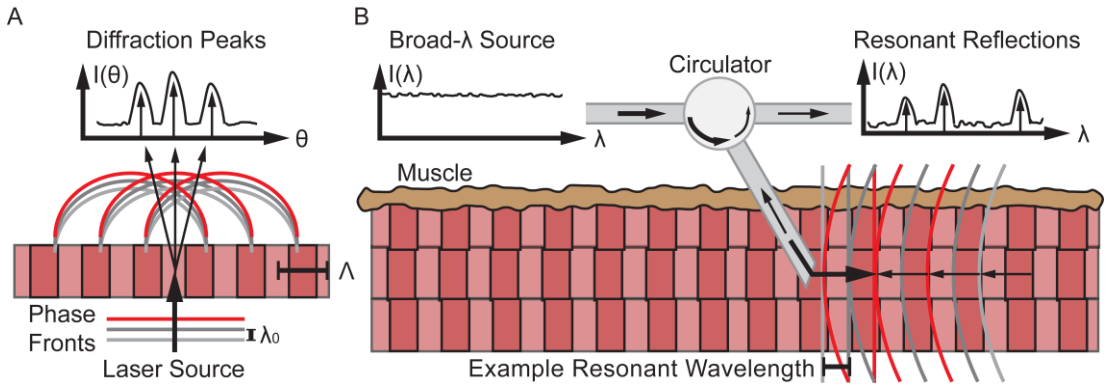

Figure 3.1: Sarcomere periodicity and illumination geometry determine optical signals. (*A*) Traditional laser diffraction method transforms sarcomere length (Λ) of a thin muscle sample into the spatial frequency domain through spatial diffraction, though a spatially encoded signal requires highly invasive surgical settings to measure sarcomere length in vivo. Red and gray lines represent the phase fronts of a laser source with wavelength λ_0. (*B*) In contrast, resonant reflection spectroscopy transforms sarcomere periodicity into the optical frequency domain through selectively reflected signals, allowing source and signal to be directed through a single minimally invasive fiber optic probe. For clarity, the phase fronts shown are from only the 4^{th} order resonant reflection.

3.2 Co-Linear Illumination to Generate Resonant Reflections

Resonant reflections occur when individual reflections originating from throughout a periodic structure constructively interfere. To a first approximation, Bragg's law, also called the Bragg resonance condition, determines which optical wavelengths will resonantly reflect from a periodic structure. Under co-linear illumination, Bragg's law states:

$$\lambda_m = \frac{2n_a\Lambda}{m} \quad (1)$$

Where λ_m is resonant wavelength for resonant order *m*; n_a is average refractive index; Λ is structure period. This expression directly links the illumination wavelengths that will resonate within the sarcomere protein structure and reflect, to sarcomere length modeled as Λ.

Bragg's law determines the resonant wavelengths, whereas Fourier decomposition of the underlying refractive index profile determines the reflection efficiency of all reflections [8, 13]. Based on the refractive index profile model used here, Fourier decomposition of a sarcomere is a superposition of four distinct protein regions:

$$n(z) = n_a + \sum_{r=1}^{4}\sum_{m} a_{r,m}\cos(2\pi mz/\Lambda) \quad (2)$$

Where $\alpha_{r,m}$ is the Fourier coefficient of region *r* and order *m*; z is distance along the long axis of sarcomeres. Each region contributes to refractive index and is prescribed by a pulse wave, so Fourier coefficients are described by [10]:

$$|a_{r,m}| = \frac{2A_r}{m\pi}\sin(m\pi L_r/\Lambda) \quad (3)$$

Where A_r is region specific index of refraction contribution; L_r is region length. Efficiency of a resonant reflection is proportional to the sum of Fourier coefficients of its harmonic order, *m* [8]. These equations have several important implications that are seen in plots of reflection efficiency generated by rigorous coupled wave analysis in the following section.

3.3 Rigorous Coupled Wave Analysis of Resonant Reflection Spectroscopy

3.3.1 Index model

Sarcomere structure was modeled as a quasi-periodic super-grating, which can be seen in electron micrographs (Fig. 3.2*A*). We used values adapted from Thornhill et al. [11], Bang et al. [14], Burkholder and Lieber [15], and Sidick et al. [16] to model the sarcomere refractive index profile. Active cross bridge cycling and skeletal muscle rigor are not included in this model because they change refractive index by less than a tenth of a percent [16].

Close examination of the sarcomere model reveals that the refractive index profile is actually a superposition of the refractive indices of four principle protein regions: m-line, z-band, myosin filaments, and actin filaments. Widths of z-band and m-line regions were 50 nm. Myosin filament length was 1.6 μm. Actin filament length was 1.1 μm unless stated otherwise. Phase of each region was matched to the sarcomere structure. Refractive index for baseline, z-band, m-line, myosin, and actin regions were 1.3473, 0.0272, 0.0200, 0.0227, and 0.0187. Importantly, overlap between actin and myosin filaments changes with sarcomere length, and refractive index profiles are adjusted accordingly (Figs. 3.2 *B*-*D*).

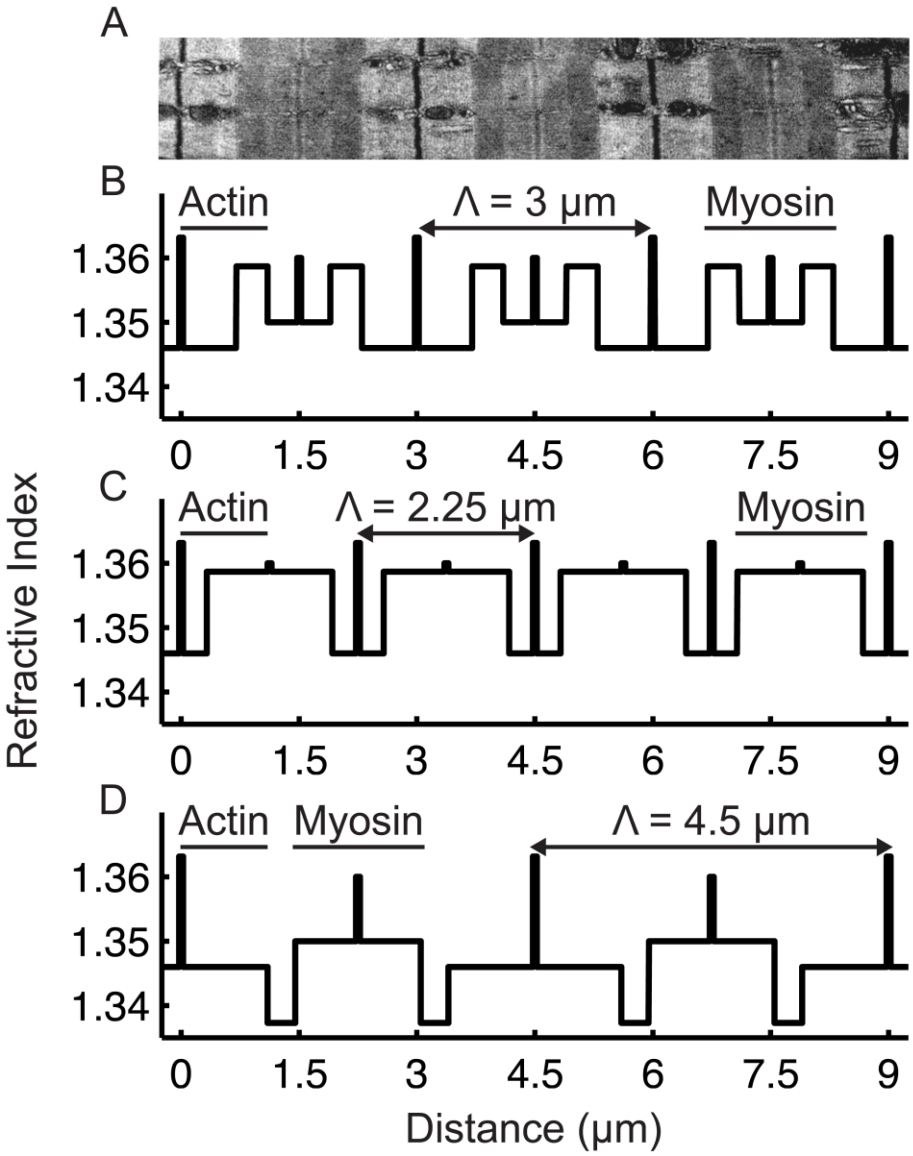

Figure 3.2: Sarcomere refractive index profile follows protein density. (*A*) An electron micrograph of sarcomeres at 3.0 μm sarcomere length (Λ) clearly shows the sarcomere protein framework, including actin and myosin filament regions. (*B-D*) Depicted are refractive index profiles corresponding to varied sarcomere lengths. Note dramatic changes in refractive index profile appearance as a function of sarcomere length.

3.3.2 Simulation

We used a one-dimensional multi-layer rigorous coupled wave analysis (RCWA) to simulate reflection spectra from sarcomeres [17]; RCWA is a widely used method for analyzing diffracting structures. Briefly, RCWA is a semi-analytical method in which periodic structures are decomposed into many layers with uniform index of refraction. Maxwell's equations are expanded by Floquet functions and a computer solves for forward and backward propagating waves. RCWA was used to calculate reflection efficiency, plotted as relative intensity, at each wavelength and sarcomere length presented.

Rather than hold sarcomere number constant, we used a constant length of 50 μm to approximate the experimental system's Rayleigh length divided by two to accommodate forward and backward paths. The illumination was collinear to sarcomeres for all simulations discussed. Sarcomere inhomogeneity was simulated by randomly varying sarcomere length for each sarcomere in series. Sarcomere length variation followed white Gaussian noise, and standard length deviations were set to approximately 60 nm to match standard deviations in sarcomere length measured by laser diffraction. All analyses were performed in MATLAB (The MathWorks, Inc., Natick, Massachusetts).

3.3.3 Results of rigorous coupled wave analysis

Fig. 3.3*A* plots reflection efficiency as a function of illumination wavelength for sarcomere length 3.0 μm. The first resonant order, where $m = 1$, is satisfied at approximately 8.5 μm; 8.5 μm is the first resonant wavelength, λ_1. λ_2 is approximately 4.2 μm and satisfies the next resonant order, $m = 2$. Note, different resonant orders are

not exactly harmonic periods, and this is caused by fine details in the sarcomere index profile. Myosin filament and m-line regions are out of phase with actin filament and z-band regions, leading to interference with the net superposition of waves giving slightly shifted peaks.

In Fig. 3.3*B*, reflection efficiency as a function of illumination wavelength and sarcomere length is represented as a contour plot. Sarcomere length equal to 3 μm is emphasized with a dashed line for comparison across Fig. 3.3. As expected from Bragg's law, resonant wavelengths appear as lines in contour plots that increase and decrease with sarcomere length, accordingly (Figs. 3.3*B*-*D*). As expected from Fourier relationships (Eq. 3), reflection efficiencies of resonant orders depend upon order and sarcomere length (Fig. 3.3*B*). Further, higher resonant orders are expected to be more sensitive to inhomogeneous sarcomere lengths in series (Figs. 3.3*C* and *D*).

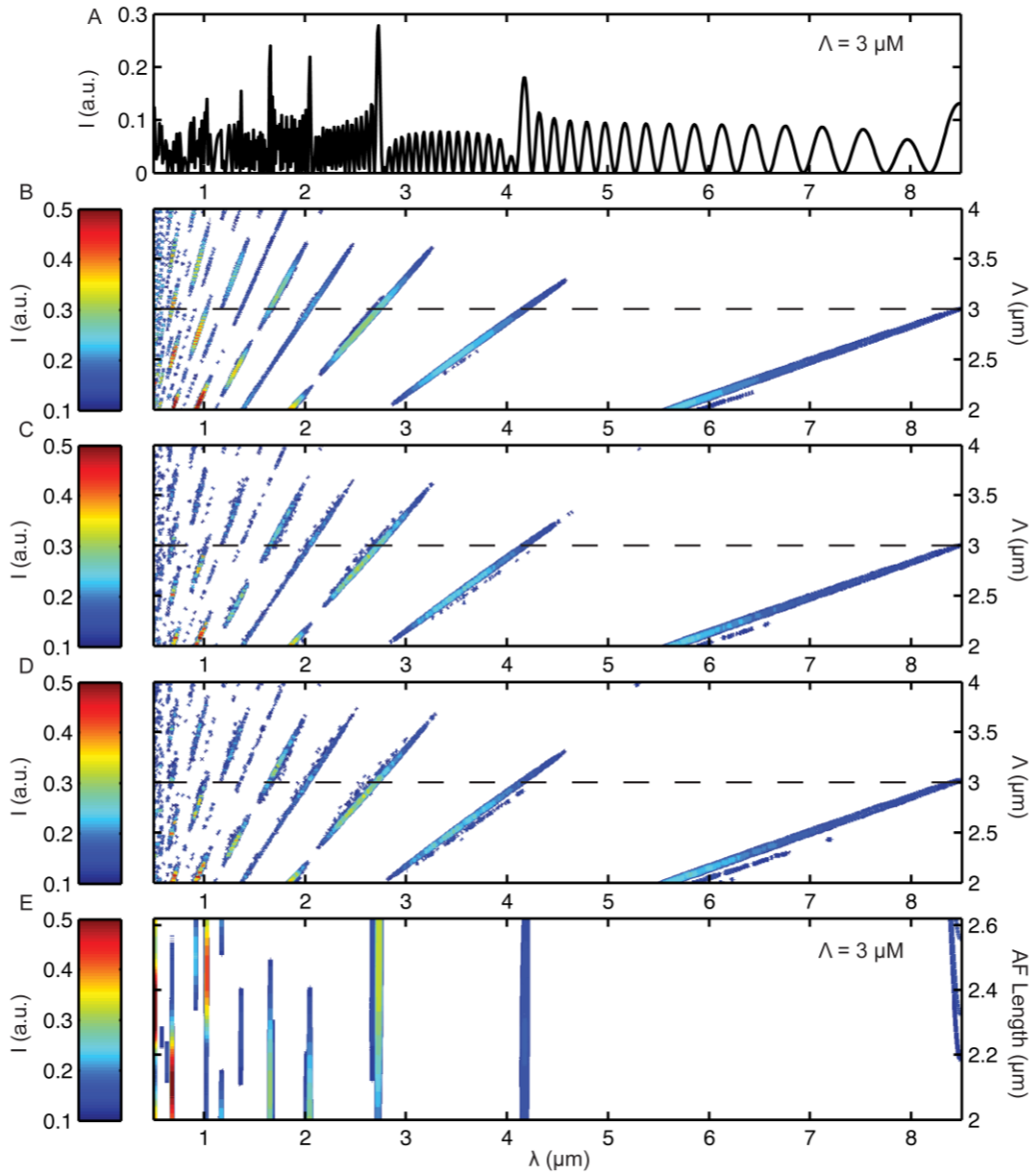

Figure 3.3: Expected reflection efficiency from sarcomeres generated by numerical simulations. (*A*) Simulated reflection efficiency as a function of wavelength for sarcomere length 3.0 μm shows a spectral fingerprint unique to this sarcomere length. (*B*) Reflection efficiency as a function of wavelength and sarcomere length is represented as a contour plot; color bar indicates reflection efficiency. Dashed line emphasizes sarcomere length 3.0 μm. (*C*) Sarcomere length inhomogeneity among sarcomeres in series introduces speckle like effects in the reflection efficiency spectrum. (*D*) 10° tilt between illumination and sarcomere long axis in the presence of sarcomere length inhomogeneity caused a slight left shift in resonant wavelengths; 12 nm was typical in wavelength range 1 to 2 μm. (*E*) Reflection efficiency varied periodically with actin filament length ranging from 1 to 1.3 μm. The grating region is twice the actin filament length due to actin spanning both sides of the z-band.

Oblique sarcomeres introduce skew to the spectral fingerprint (Fig. 3.3*D*). A 10° tilt of the probe, which is easily recognizable experimentally, would result in less than 25 nm short-estimate of sarcomere length (Eq. 1) for the wavelength ranges used herein; tilt affects are likely less that natural sarcomere length variability. Still, tilt was carefully minimized in all experiments herein. Lastly, reflection efficiencies are predicted to be periodic with actin filament lengths (Eq. 3 and Fig. 3.3*E*), which is an important consideration when considering different muscles and species [15]. In many optical applications, only fundamental resonant reflections (λ_1) are measured or studied. However, since sarcomere length varies by more than a factor of two, locating a single resonant wavelength in a spectrum of reflected light does necessarily enable solving for sarcomere length because the resonance may originate from neighboring harmonic orders. Consequently, a wide spectrum that crosses at least two resonant orders is needed to measure a sufficient spectral fingerprint to uniquely calculate sarcomere length. Importantly, this statement is different than claiming two resonant reflections are required. For example, the 4^{th}, 5^{th}, and 6^{th} orders are located in the wavelength range 1 μm to 2 μm and sarcomere length range 2.7 μm to 2.8 μm, but the 5^{th} and 6^{th} orders reflection intensity have disappeared (Figs. 3.3*B-D*). So, sarcomere length of 2.75 μm is predicted to yield a single resonant reflection using RRS. Still, this fingerprint is unique to this sarcomere length and wavelength range, and so sarcomere length can be calculated with confidence from a single measured resonant wavelength falling in this wavelength band.

Therefore, bandwidth of an experimental system must satisfy the need to envelop multiple predicted resonant orders. Resonant orders that have weak reflections satisfy this

requirement if at least one resonant order is measurable for all sarcomere lengths. On one hand, higher orders cover a smaller wavelength range, enabling more orders to be measured (Fig. 3.3). On the other hand, higher orders are affected more significantly by sarcomere inhomogeneity and length changes (Fig. 2*B-E*). To balance these trade-offs, we identify the 4^{th}, 5^{th}, and 6^{th} orders as most promising for experimental measurement.

3.4 Three Dimensional Simulations and Optical Probe Coupling

Resonant reflection spectroscopy requires collinear illumination of skeletal muscle sarcomeres. As such, an optical probe must be used to deliver and collect light in vivo. The simplest such device, which is as small as possible to reduce tissue damage, is a lensed fiber optic. Exact sarcomere orientation during an in vivo experiment may not be known. So, the relative tilt between the fiber optic probe and sarcomeres is unknown. To estimate in vivo application of RRS with a lensed fiber optic and the extent of the effect of tilt misalignments between probe and sarcomeres, we extended our computational models to three dimensions by applying a finite difference time domain (FDTD) method to solve propagating electromagnetic fields. Simulations show the importance of illumination geometry in both idealized and realistic probe and sarcomere geometries.

3.3.4 Three dimensional simulation environment

We performed the FDTD method in computer simulations in Matlab (The MathWorks, Inc., Natick, Massachusetts) and openEMS [18] software packages. FDTD solves Maxwell equations in a linearized form where only nearest-neighbor interactions

need to be considered in incremental discrete time steps of voxels through the geometrical model [19]. This treatment offers the significant advantage of arbitrary model geometry, and it was chosen due to the distinct geometry differences between fiber optic and sarcomeres. The lensed fiber optic was simulated with parameters to match a lensed single mode fiber (SMF28) with a lensed geometry to create 10μm spot diameter. The core and cladding index of refraction were 1.45204 and 1.44681, respectively. Index of refraction values for all of the sarcomere protein regions match as discussed before. Simulations were performed across 0, 5, 10, and 15 degrees of tilt between fiber optic and sarcomere long axes. Simulations either used idealized sarcomeres at 3 μm length or sarcomeres with phase misalignments at 3 μm length and 5% coefficient of variation.

3.4.5 Results: three dimensional simulations with finite difference time domain method

Electric field plots exhibit propagations paths and spot size as expected (Fig. 3.4). Interestingly, a small degree of diffraction can be seen regardless of tilt angle. Simulated reflection spectra from idealized sarcomeres show resonant peaks at approximately 1.35 and 1.62 μm and match with previous RCWA results (Fig. 3.5A). Including a fiber optic adds the additional complexity of coupling reflected light into the fiber core (Figs. 3.5 B and C). Although reflection efficiency is still strong at 10 degrees of misalignment (Fig. 3.5A), coupling efficiency into the fiber optic core and therefore signal strength drops more than a factor of 3 (Figs. 3.5 B and C). Misalignments of at least 15 degrees completely destroy the resonant reflection spectrum and signal (Fig. 3.5), though a misalignment of 10 degrees is easily recognizable in practice.

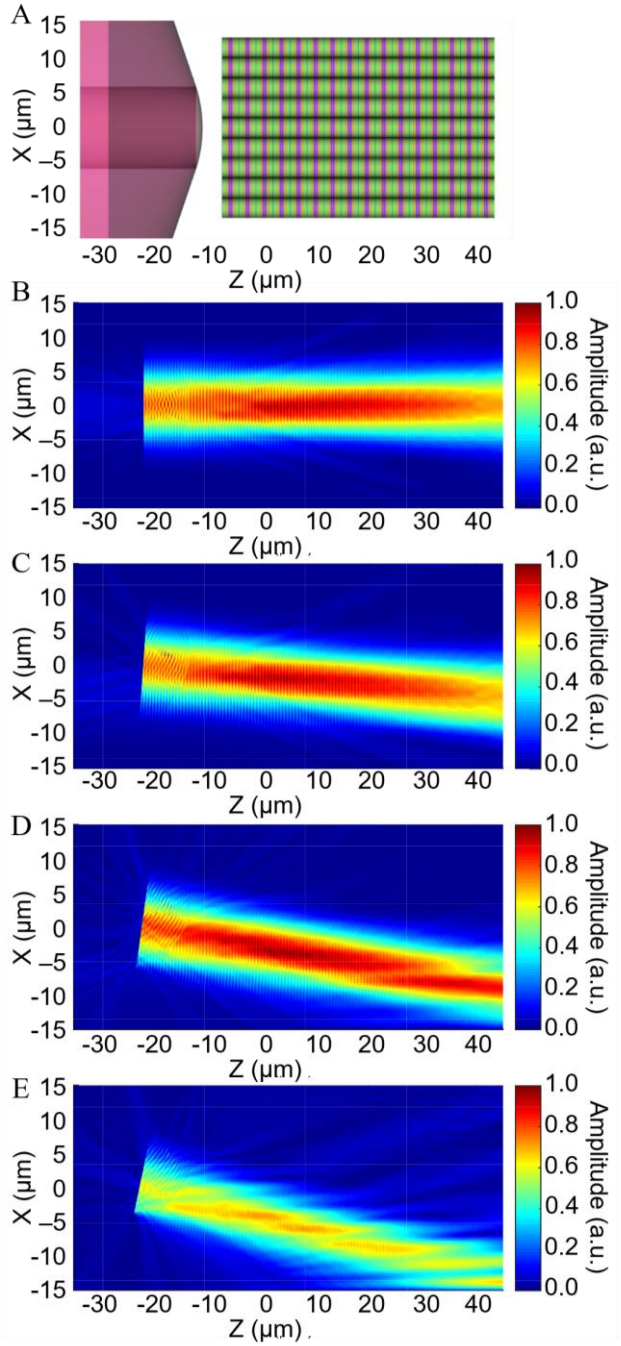

Figure 3.4: Three dimensional finite difference time domain simulations of sarcomere geometry and beam propagation from an optical probe are used to estimate reflection collection efficiency. (*A*) Simulation geometry of 3μm sarcomere length at 0 degrees tilt. (*B-E*) Electric field propagation for 0, 5, 10, and 15 degree tilts, respectively

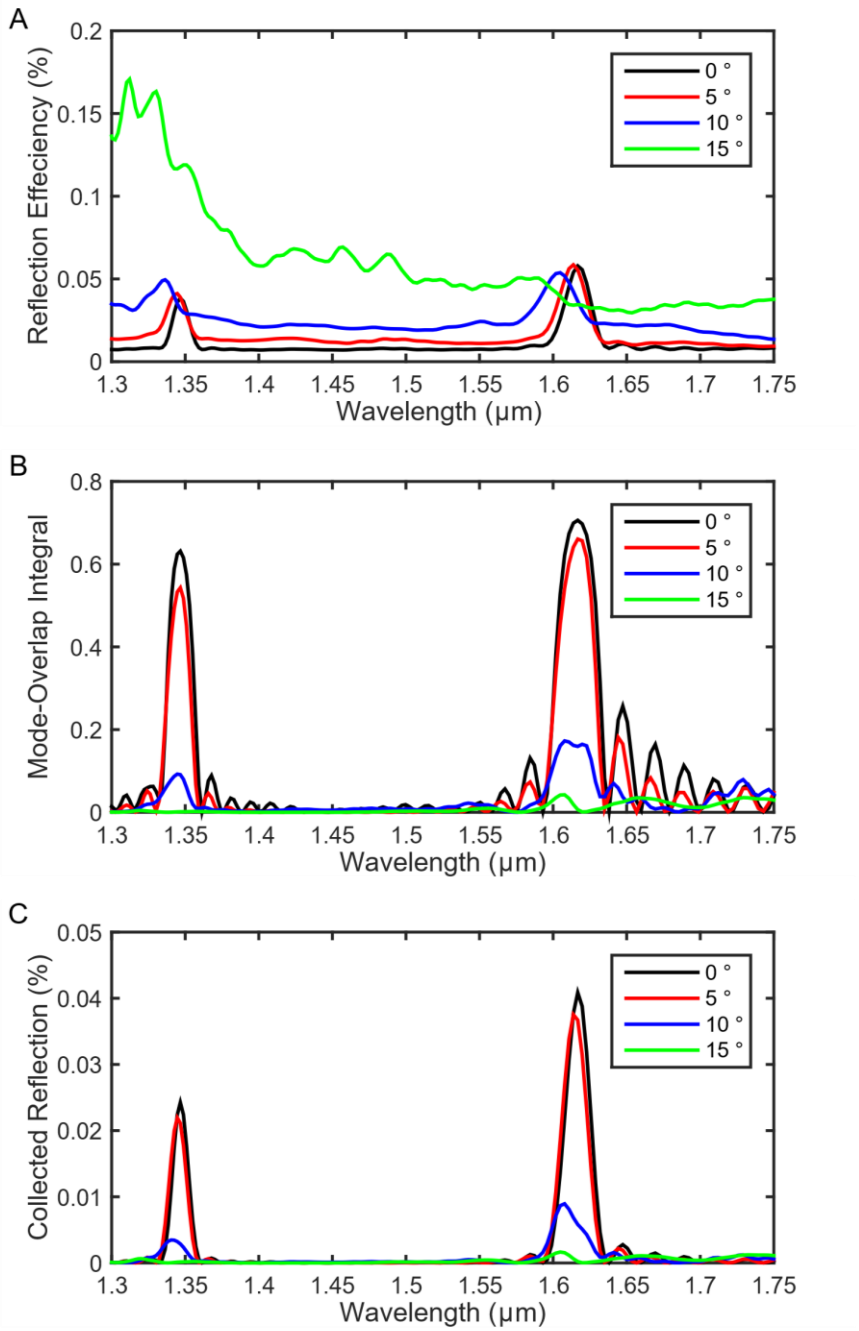

Figure 3.5: Collection of reflected spectra is dramatically reduced at larger than five degrees of tilt between the long axes of sarcomeres and the optical probe for idealized sarcomeres with 3 μm length. (*A*) Raw reflection spectra from sarcomeres integrated from cross-sections. (*B*) Mode-overlap integral for coupling into the optical probe at varying degrees of tilt. (*C*) Reflection spectra measured by the optical probe.

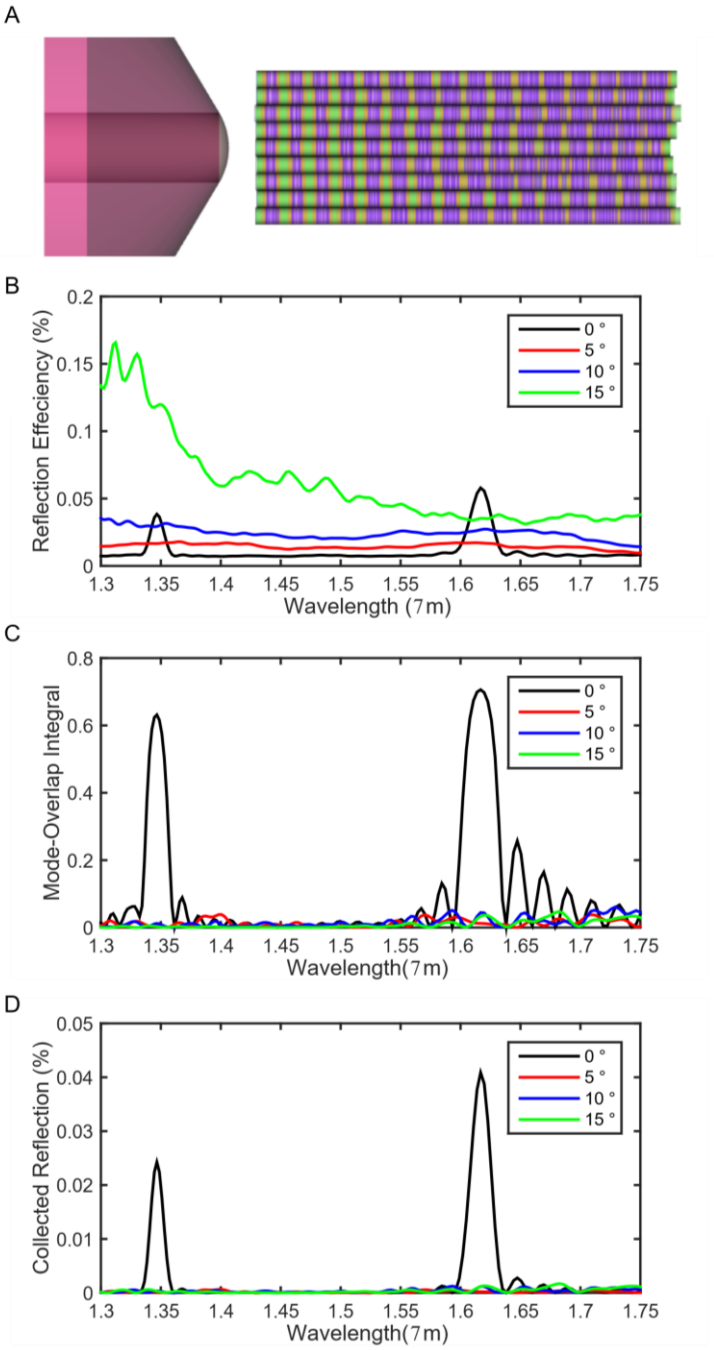

Figure 3.6: Simulations of misaligned and heterogeneous sarcomeres highlight the importance of collinear illumination to the long axes of sarcomeres. (*A*) Simulation geometry of 3µm sarcomere length with 5% coefficient of variation at 0 degrees tilt. (*B*) Raw reflection spectra from sarcomeres integrated from cross-sections. Resonance is destroyed for tilts above 0 degrees (*C*) Mode-overlap integral for coupling into the optical probe at varying degrees of tilt. (*D*) Reflection spectra measured by the optical probe.

Simulations of heterogeneous sarcomeres with a reasonable 5% coefficient of variation show critical importance of collinearity between probe and sarcomeres. Under these conditions, resonant spectra are destroyed at misalignments as low as 5 degrees (Fig. 3.6). Interestingly, collinear illumination appears insensitive to heterogeneous sarcomeres.

3.5 Conclusion

Computer simulations of the proposed resonant reflection spectroscopy method highlight several considerations. First, broad wavelength illumination is required to distinguish between degenerate solutions to Bragg's law. Second, sarcomere length heterogeneity may not dramatically alter the location of resonant peaks, and so resonant peaks can be used to calculate sarcomere length despite secondary peaks appearing in the spectrum. Third, collinear illumination is critical to generating strong signals, particularly when using small fiber optics probes. The next section demonstrates experimental proof of concept for resonant reflection spectroscopy to measure sarcomere length.

3.6 Acknowledgements

Chapter 3 is, in part, nearly identical to sections of a peer reviewed article entitled "Resonant reflection spectroscopy of biomolecular arrays in muscle" by Young KW, Radic S, Myslivets E, O'Connor SM, and Lieber RL. The article was published in *Biophysical Journal* 2014, 107(10):2352-2360. This work was funded by the Department of Veteran's Affairs Grant A9028R and NIH Grant R24 HD050837. K.W.Y., S.R., and

R.L.L. have disclosed these findings to the University of California San Diego Technology Transfer Office.

3.7 References

1. Cleworth D, Edman K: **Changes in sarcomere length during isometric tension development in frog skeletal muscle**. *J Physiol* 1972, **227**:1–17.

2. Lieber RL, Loren GJ, Fridén J: **In vivo measurement of human wrist extensor muscle sarcomere length changes.** *J Neurophysiol* 1994, **71**:874–81.

3. Ward S, Takahashi M, Winters T, Kwan A, Lieber R: **A novel muscle biopsy clamp yields accurate in vivo sarcomere length values**. *J Biomech* 2009, **42**:193–196.

4. Llewellyn ME, Barretto RPJ, Delp SL, Schnitzer MJ: **Minimally invasive high-speed imaging of sarcomere contractile dynamics in mice and humans.** *Nature* 2008, **454**:784–8.

5. Cromie MJ, Sanchez GN, Schnitzer MJ, Delp SL: **Sarcomere lengths in human extensor carpi radialis brevis measured by microendoscopy.** *Muscle Nerve* 2013, **48**:286–92.

6. König K, Becker TW, Fischer P, Riemann I, Halbhuber KJ: **Pulse-length dependence of cellular response to intense near-infrared laser pulses in multiphoton microscopes.** *Opt Lett* 1999, **24**:113–5.

7. Kogelnik H: **Coupled wave theory for thick hologram gratings**. *Bell Syst Tech J* 1969, **48**:2909–2947.

8. Erdogan T: **Fiber grating spectra**. *J Light Technol* 1997, **15**:1277–1294.

9. Born M, Wolf E: *Principles of Optics*. 2nd edition. *Volume 1*. New York, NY: Pergamon Press; 1999.

10. Gray RM, Goodman JW: *Fourier Transforms: An Introduction for Engineers*. Kluwer Academic Publishers Norwell, Massachusetts; 1995.

11. Thornhill RA, Thomas N, Berovic N: **Optical diffraction by well-ordered muscle fibres.** *Eur Biophys J* 1991, **20**:87–99.

12. Yang X, Lorenser D, McLaughlin R a, Kirk RW, Edmond M, Simpson MC, Grounds MD, Sampson DD: **Imaging deep skeletal muscle structure using a high-sensitivity ultrathin side-viewing optical coherence tomography needle probe.** *Biomed Opt Express* 2013, **5**:136–48.

13. Goodman JW: *Introduction to Fourier Optics*. Roberts and Company Publishers, Colorado; 2005.

14. Bang M-L, Li X, Littlefield R, Bremner S, Thor A, Knowlton KU, Lieber RL, Chen J: **Nebulin-deficient mice exhibit shorter thin filament lengths and reduced**

contractile function in skeletal muscle. *J Cell Biol* 2006, **173**:905–16.

15. Burkholder TJ, Lieber RL: **Sarcomere length operating range of vertebrate muscles during movement**. *J Exp Biol* 2001, **204**(Pt 9):1529–1536.

16. Sidick E, Baskin RJ, Yeh Y, Knoesen a: **Rigorous analysis of light diffraction ellipsometry by striated muscle fibers.** *Biophys J* 1994, **66**:2051–61.

17. Moharam MG, Grann EB, Pommet DA, Gaylord TK: **Formulation for stable and efficient implementation of the rigorous coupled-wave analysis of binary gratings**. *J Opt Soc Am A* 1995, **12**:1068.

18. Liebig T: **openEMS - Open Electromagnetic Field Solver**. .

19. Kunz KS, Luebbers RJ: *The Finite Difference Time Domain Method for Electromagnetics*. CRC Press; 1993.

Chapter 4 In vitro proof of concept for resonant reflection spectroscopy

4.1 Introduction

Resonant reflection spectroscopy (RRS) requires wide optical bandwidth to solve the degenerate nature of the Bragg grating equation (Chapter 3). Conventional optical sources, however, are limited to optical wavelengths that correspond to electron energy transitions of available materials. As such, they offer insufficient optical bandwidth to perform RRS across the full range of potential sarcomere lengths found in animals and humans [1]. In order to perform a proof of concept experiment that assesses agreement between RRS estimates and transmitted laser diffraction estimates of sarcomere length, we built a custom optical system to fit this need.

Based upon results from computer simulations, we built a custom supercontinuum source [2] with 800 nm optical bandwidth and tested feasibility of RRS on ten muscles. We compared measured RRS spectra to predicted RRS spectra from idealized sarcomeres, and compared sarcomere lengths measured by RRS and LD. From these comparisons, we conclude that RRS successfully captures sarcomere length, though several engineering challenges remain to extend RRS for desired in vivo use.

4.2 Materials and Methods

4.2.1 Tissue preparation

Whole hind limbs were collected from euthanized mice and rabbits sacrificed for other research. Then, limbs were pinned to cork board and chemically fixed in 10% formalin for two days. Each sample was rinsed and stored in phosphate buffered saline. Whole tibialis anterior (TA) and extensor digitorum longus (EDL) muscles were

collected. Three small subsamples were microdissected at the middle third from each whole muscle for sarcomere length measurement by laser diffraction. Then, muscles were cut in half at approximately 15 degrees from normal. This facilitated coupling between the slanted face of the optical probe and muscle fibers by ensuring the optical path difference across surfaces was close to zero.

4.2.2 Supercontinuum source

A custom system was used to generate a supercontinuum source (Fig. 4.1*A*). Briefly, a Mach-Zehnder modulator (MZM) was used to generate optical pulses that were optically amplified to 1 W power and sent into 280 m of highly nonlinear fiber (HNLF; Sumitomo Electronics, Japan) with 1550 nm zero dispersion wavelength [4]. The optimal spectrum (Fig. 4.1*B*) was generated using these pulse characteristics: 1553.4 nm center wavelength (HP 81684 tunable laser, Palo Alto, California), 25 ns pulse duration, and 1 MHz repetition rate. The raw supercontinuum spectrum at the output of the HNLF spanned 800 nm with total power in excess of 500 mW. Three wavelength division multiplexers (*WDM*s) were used to divide the supercontinuum spectrum into three wavelength bands; each band used had final output power less than 15 mW and 3dB flatness.

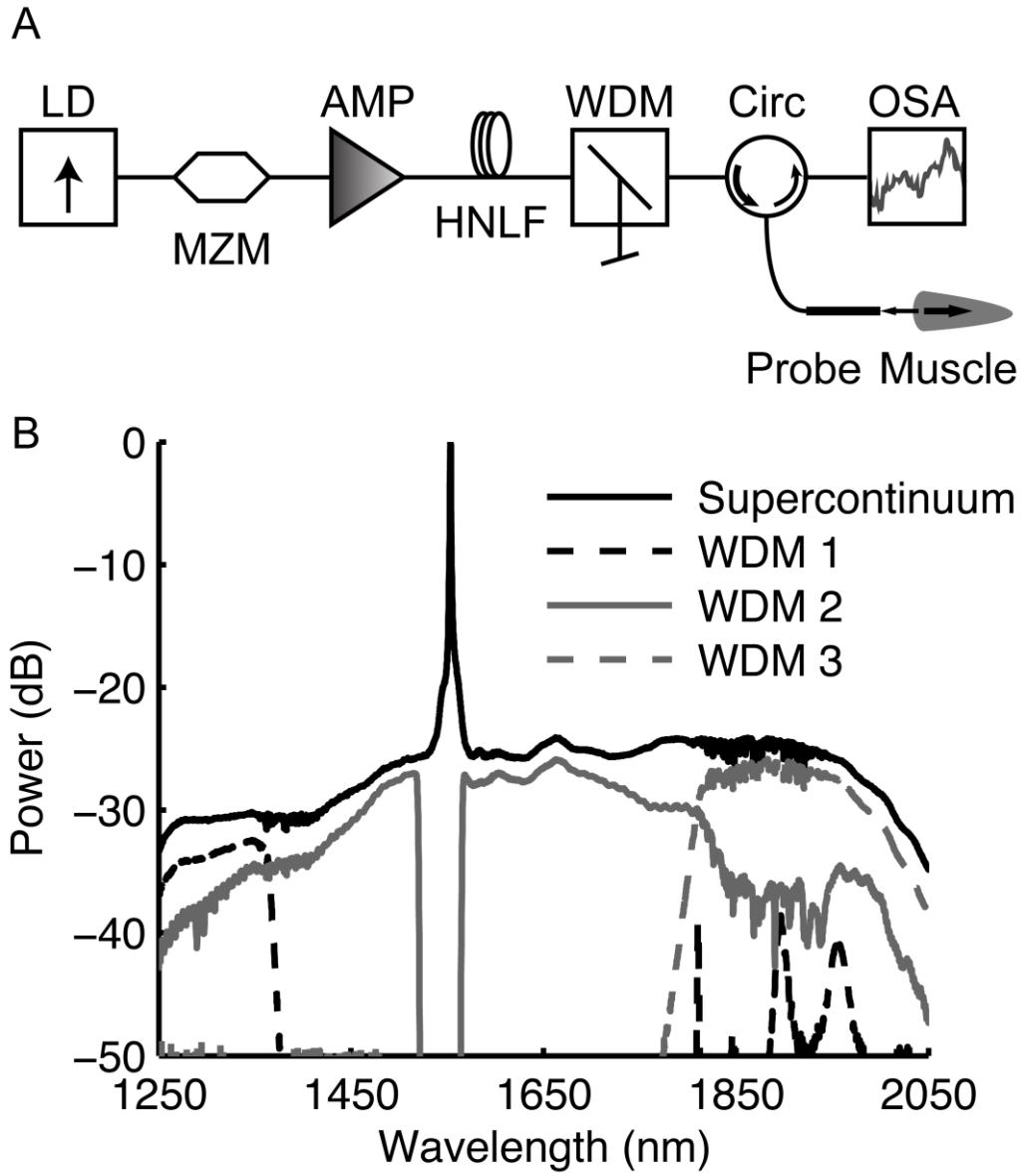

Figure 4.1: (*A*) Schematic of supercontinuum spectroscopic system. Abbreviations are as follows: LD, laser diode; MZM, Mach-Zehnder modulator; AMP, optical amplifiers; HNLF, highly nonlinear fiber; WDM, wavelength division multiplexer; Circ, circulator; OSA, optical spectrum analyzer. (*B*) Supercontinuum spectroscopy system output before and after wavelength division multiplexing.

4.2.3 Sarcomere length measurement by laser diffraction

Small subsamples were placed on glass slides and trans-illuminated with a 10 mW He-Ne laser with 633 nm center wavelength. Resulting diffraction patterns illuminated a

frosted glass slide, and distances between diffracted peaks were measured with digital calipers. The measurement system was calibrated using a wire grating with 2.0 μm period. Sarcomere length was calculated from the distance measurements and calibration [3]; sarcomere length measurement from this system had a typical standard deviation of approximately 60 nm and ranged from 2.36-3.03 μm.

4.2.4 Sarcomere length measurement by resonant reflection spectroscopy

Muscle samples were placed on a stage, and the middle of the cross-sectional face of muscle was co-linearly aligned to the optical probe. Thus, sarcomeres close to the middle of the muscle were measured by RRS. The probe, a single mode fiber patch cable terminated with angled plain connectors, illuminated muscle fibers and collected reflected power. An optical circulator, which only permits light propagation to forward ports, directed supercontinuum source illumination through the probe and directed reflected signals to an optical spectrum analyzer (OSA; Yokogawa AQ6375, Japan) that measured reflected power spectra (Fig. 4.1*A*).

The number of sarcomeres measured by RRS in series and in parallel is affected by scattering and beam coupling characteristics of the optical probe. Photon mean free paths in muscle tissue are roughly millimeters in length [5], whereas the Rayleigh length of the optical probe is at least an order of magnitude shorter. Based upon a myofibril (sarcomere) diameter of 1 μm and beam parameters derived from a 0.14 NA optical probe, we estimate that approximately 1500 sarcomeres contributed to the RRS signal.

Resonant wavelengths (maximal reflections) were automatically selected from measured spectra. Two resonant wavelengths were measured in eight of ten muscles. In

one muscle, a single resonant wavelength was present within the measurement window, which is consistent with theory for particular sarcomere lengths (see Chapter 3). In another muscle, three resonant wavelengths were measured. Sarcomere lengths were calculated using the following procedure. First, one measured resonant wavelength was used to generate a set of possible sarcomere lengths based upon varying harmonic orders. Then, the measured spectrum was compared with predicted spectral "fingerprints" to identify possible sarcomere lengths.

Sarcomeres within real muscles are not homogenous. After solving for resonant orders using the procedure described above, sarcomere length was calculated for each measured resonant wavelength to account for natural variability. These sarcomere length estimates were averaged to generate the sarcomere lengths presented. For more details regarding relationships between resonant wavelengths and sarcomere lengths, see Chapter 3.

4.2.5 Statistical analysis

Linear correlations were performed in MATLAB (The MathWorks, Inc., Natick, Massachusetts) and data points were treated as independent samples. A paired t-test was performed to compare average isometric force before and after probe insertion using Prism software (GraphPad, San Diego, California). Power analyses were performed using G*Power 3.1 [6] (Heinrich Heine University Dusseldorf, Germany). Significance level was set to 0.05 for all tests.

4.3 Results

4.3.1 Experimentally measured vs. simulated resonant reflections

To test our model, we measured multiple resonant orders from muscles of known sarcomere length using the new supercontinuum spectroscopy system and then compared measurements to numerical simulations. In ten muscles, experimental measurements agreed remarkably well with simulations.

Overlay of unprocessed reflected power and theoretical simulations from muscle tissue with sarcomere length 2.45 μm exhibit agreement (Figs. 4.2 *A* and *B*). Importantly, the resonant wavelengths, which have the strongest reflections, match extremely well for both the 4^{th} and 5^{th} order. In this example, average difference between simulated resonant wavelength from idealized sarcomeres and experimental measurements was 3.5 nm, which equates to a 6.5 nm sarcomere length or 0.27% uncertainty. Furthermore, the reflection spectrum approximates a superposition of sinc functions as predicted by the theoretical model [7, 8]. Notably, the period of oscillations in measured spectra roughly match the predicted period.

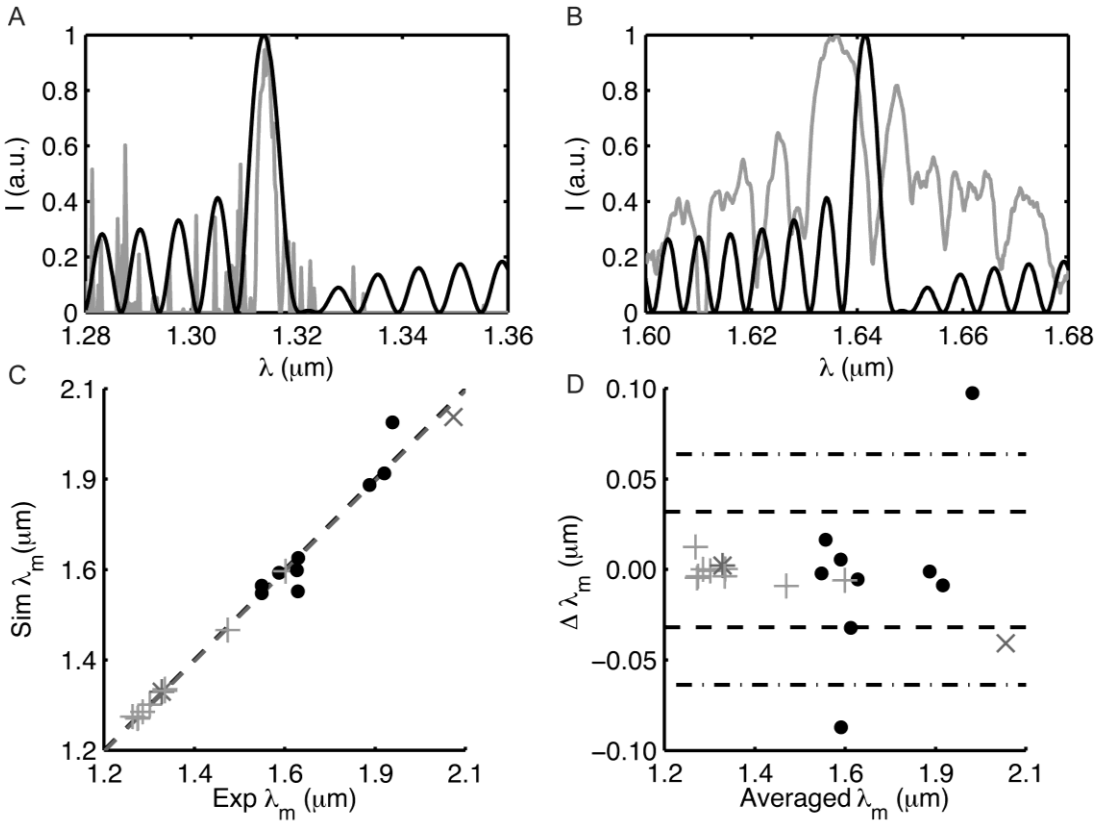

Figure 4.2: Theory for sarcomere refractive index accurately models reflected signals across all muscles tested (N = 10). (*A* and *B*) Overlay of simulated (*black*) and experimentally measured (*gray*) reflection spectra from muscle with 2.45 μm sarcomere length for 5th (*A*) and 4th (*B*) order resonances. Wavelength ranges are focused near resonant wavelengths to show nm-scale detail. (*C*) Experimentally measured and simulated resonant wavelengths (λ_m) for 3rd order (X), 4th order (•), 5th order (+), and 6th order (*) significantly correlate (R^2 = 0.984, $p < 0.001$) across muscle samples. Dashed line represents line of unity. (*D*) An agreement plot presents an unbiased view of variability in differences ($\Delta\lambda_m$) between simulated and experimentally measured resonant wavelengths. Dashed lines represent standard deviation and twice the standard deviation. There is no systematic bias between modeled and experimentally measured resonances (P = 0.86).

Experimental measurements match well across the entire sample, which includes a range of sarcomere lengths from 2.36 to 3.03 μm. This dataset revealed a significant correlation ($p < 0.001$) between experimentally measured and simulated resonant wavelengths with the theoretical model explaining 98% (R^2 = 0.984) of the variability in experimental measurements (Fig. 4.2*C*). As a further test, we generated an agreement plot

to visualize the fit between data sets (Fig. 4.2*D*). Agreement plots are not visually biased by scale as can occur with correlations [9]. In the agreement plot, we easily see that two of the ten muscles are less accurately modeled by idealized sarcomeres. Currently, we lack sufficient data to conclude the cause of disagreement in these muscles, but we hypothesize, based upon numerical simulations, that the shifts are caused by radial and/or longitudinal sarcomere length inhomogeneity. Nonetheless, these shifts do not prevent sarcomere length measurements, as seen in the next section.

4.3.2 Sarcomere length measured by laser diffraction vs. resonant reflection spectroscopy

Using the procedure described in Methods, we calculated sarcomere length from RRS measurements. Sarcomere length measured by LD and RRS were highly significantly correlated ($R^2 = 0.984$, $p < 0.001$) (Fig. 4.3*A*). Variability between measurement methods is more clearly seen in an agreement plot (Fig. 4.3*B*). Differences between method sarcomere length measurements were not significantly correlated across sarcomere length ($P = 0.16$), indicating sarcomere lengths measured by RRS are not systematically biased (80% power to detect 1.7 nm/μm skew). Even with a one-dimensional and idealized sarcomere model, sarcomere lengths measured by RRS and LD agree with a standard deviation of ±35 nm (Fig. 4.3*B*), well within a physiologically meaningful tolerance.

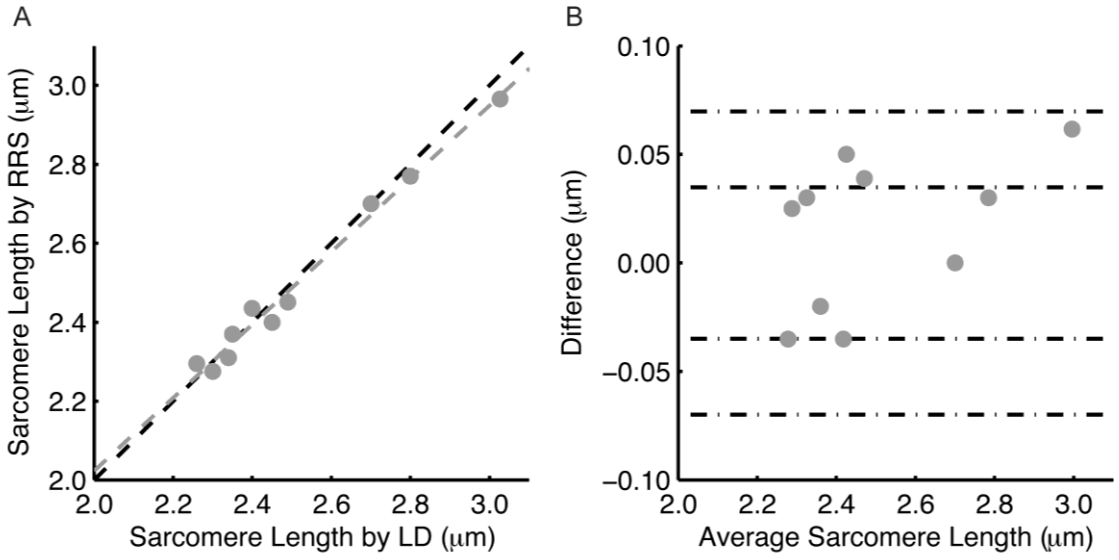

Figure 4.3: (*A*) Sarcomere lengths measured by LD and RRS significantly correlate ($R^2 = 0.984$, $p < 0.001$). Black Dashed line represents line of unity. Gray dashed line represents line of best fit. (*B*) Agreement plot revels no systematic bias in sarcomere length measurements by RRS ($P = 0.16$).

4.4 Discussion

This study demonstrates two key points: theoretical development of RRS and experimental assessment of its ability to measure sarcomere length. RRS can potentially enable critically important sarcomere length measurements in vivo, in real time, and in humans because the information is encoded in optical wavelengths rather than spatial information as is the case in current techniques [10, 11]. Using a new supercontinuum system and a one-dimensional sarcomere refractive index model, we demonstrated that sarcomere lengths measured by RRS agree remarkably well with sarcomere lengths measured by LD, a standard technique. We conclude that RRS is theoretically feasible, though several key points differentiate the feasibility system used here and the desired in vivo RRS technique. A number of considerations are raised in the following discussion,

but still, the idealized model of sarcomeres explained 98% of the variability in the key information contained in measured RRS spectra.

First, an extra-muscular probe was used in the feasibility experiment. This allowed us to explore illumination angles to align illumination with the long axes of sarcomeres and provide confidence relating the theoretical model with experimental geometry. Severely oblique sarcomeres would have demanded data collection and alignment tests beyond the scope of this initial feasibility study. A future intramuscular probe may not have control of illumination angles and more work is necessary to determine if redundant measurements are needed to address this added level of complexity, however, simulations of 10° oblique sarcomeres caused skew in the spectral fingerprint that would change sarcomere length estimates by less than 25 nm. Additionally, intramuscular probes impose geometric changes to the local muscle fibers, though these changes appear small in histological analysis.

Second, chemically fixed muscles were used for RRS measurements while the true benefit of RRS will come from in vivo use. Using fixed muscles allowed us to prototype the experiments while minimizing the animals needed for this study. Importantly, we recently demonstrated [12] that fixation does not systematically introduce errors in sarcomere length measurements by LD. Signal generation in RRS and LD are fundamentally similar, though the geometry is different, so it is unlikely that fixation dramatically confounded the results. Fixation, though, may systematically change baseline refractive index compared to fresh muscle sarcomeres. This may cause a corresponding shift to measured sarcomere lengths. Refractive indexes used here led to

RRS measured sarcomere lengths to match those measured by LD in fixed muscles, though a baseline shift may be required for in vivo use.

Third, in vivo measurements are associated with natural movement. Motion artifacts are a confounding factor present in microendoscopy measurements of in vivo sarcomere length because the technique operates at only a few Hz [11, 13]. RRS, however, does not require point scanning and can operate at many kHz rates. Thus, motion artifacts will not confound sarcomere length data collected by RRS. If index of refraction changes during contraction are minimal or can be resolved, RRS may offer a unique capability to even distinguish between passively and actively contracting muscle, in vivo. More engineering and experiments are required to test these hypotheses.

Last, several other factors may systematically affect RRS signals and have not been included in the current model. Concentration changes in non-contractile organelles, such as mitochondria and nuclei, may affect the base level refractive index and systematically shift sarcomere lengths shorter or longer. We expect, however, that the magnitudes of these affects will be buried by variability caused by within-muscle sarcomere length heterogeneity. Length changes to z-band or actin filament regions affect the sarcomere refractive index profile and are expected to affect the relative intensities of resonant orders. The extent to which this is a confounding factor or meaningful data is currently unknown and should be a topic of future investigation.

4.5 Conclusions

RRS offers a potential breakthrough for in vivo sarcomere length data collection because it is not restricted by the same fundamental limitations as current techniques. Using the theoretical framework presented here, we accurately predicted the resonant reflections that arise from muscle sarcomeres. Notably, we demonstrated that sarcomere lengths measured by RRS matched those measured by traditional LD. Engineering challenges, such as developing appropriate laser sources and optical probes, remain to extend RRS in vivo, but these results demonstrate the feasibility of RRS and point to promising future applications.

4.6 Acknowledgements

Chapter 4 is nearly identical to sections of a peer reviewed article entitled "Resonant reflection spectroscopy of biomolecular arrays in muscle" by Young KW, Radic S, Myslivets E, O'Connor SM, and Lieber RL. The article was published in *Biophysical Journal* 2014, 107(10):2352-2360. This work was funded by the Department of Veteran's Affairs Grant A9028R and NIH Grant R24 HD050837. K.W.Y., S.R., and R.L.L. have disclosed these findings to the University of California San Diego Technology Transfer Office.

4.7 References

1. Burkholder TJ, Lieber RL: **Sarcomere length operating range of vertebrate muscles during movement**. *J Exp Biol* 2001, **204**(Pt 9):1529–1536.

2. Dudley JM, Taylor JR: **Ten years of nonlinear optics in photonic crystal fibre**. *Nat Photonics* 2009, **3**:85–90.

3. Lieber RL, Yeh Y, Baskin RJ: **Sarcomere length determination using laser diffraction. Effect of beam and fiber diameter.** *Biophys J* 1984, **45**:1007–16.

4. Birks TA, Wadsworth WJ, Russell PSJ: **Supercontinuum generation in tapered fibers**. *Opt Lett* 2000, **25**:1415–1417.

5. Xia J, Weaver A, Gerrard DE, Yao G: **Monitoring sarcomere structure changes in whole muscle using diffuse light reflectance.** *J Biomed Opt* 2012, **11**:040504.

6. Dupont WD, Plummer WD: **Power and sample size calculations for studies involving linear regression.** *Control Clin Trials* 1998, **19**:589–601.

7. Erdogan T: **Fiber grating spectra**. *J Light Technol* 1997, **15**:1277–1294.

8. Gray RM, Goodman JW: *Fourier Transforms: An Introduction for Engineers*. Kluwer Academic Publishers Norwell, Massachusetts; 1995.

9. Bland JM, Altman DG: **Statistical methods for assessing agreement between two methods of clinical measurement**. *Int J Nurs Stud* 2010, **47**:931–936.

10. Cleworth D, Edman K: **Changes in sarcomere length during isometric tension development in frog skeletal muscle**. *J Physiol* 1972, **227**:1–17.

11. Llewellyn ME, Barretto RPJ, Delp SL, Schnitzer MJ: **Minimally invasive high-speed imaging of sarcomere contractile dynamics in mice and humans.** *Nature* 2008, **454**:784–8.

12. Ward S, Takahashi M, Winters T, Kwan A, Lieber R: **A novel muscle biopsy clamp yields accurate in vivo sarcomere length values**. *J Biomech* 2009, **42**:193–196.

13. Cromie MJ, Sanchez GN, Schnitzer MJ, Delp SL: **Sarcomere lengths in human extensor carpi radialis brevis measured by microendoscopy.** *Muscle Nerve* 2013, **48**:286–92.

Chapter 5 Real-time in vivo sensing of muscle protein structure

5.1 Introduction

Bench-top models and single time point biopsies are insufficient to understand complex biology. In the past decade, however, the use of optical technology to define tissue structure and detect disease has increased dramatically. Thanks to recent breakthroughs, it is possible to measure cellular structures with sufficient resolution to access cell function and maintain this resolution across many millimeters to generate data relevant to tissue function[1, 2]. Yet, techniques that are compatible with other target organs and general minimally-invasive use remain challenging. Here we describe a new minimally invasive optical approach that uses a 250 μm fiber optic probe and can acquire data at kHz rates with nm length resolution across mm distances during movement and activity. Additionally, we access the amount of damage caused by inserting the fiber optic probe. Histology of cross-sections of muscle tissue where probes have been inserted show minimal damage. Muscular force before and after probe insertion are not different. Our method uses a combination of resonant reflection spectroscopy (RRS), which determines tissue microstructure, and optical frequency domain interferometry (OFDI), which controls and measures the precise depth at which the signal is obtained. For the first time, we show analysis of the optical reflections from muscle tissue that easily captures submicron submillisecond movement of muscle proteins, creating the potential for an entirely new approach to understand movement disorders in patients with muscle dystrophy, Parkinson's disease, stroke or cerebral palsy. It's likely this method will be

performed during voluntary movement, which sets it apart from all other tissue measuring methods developed to date.

5.2 In Vivo Optical Probe Insertion Causes Minimal Sarcomere Damage

5.2.1 Muscle biomechanics system

TA muscles were chosen for accessibility and availability of reference data [3]. All procedures were performed with the approval of the Institutional Animal Care and Use Committee (IACUC). Isometric force measurement and animal preparation followed previously described methods [4, 5], but the anterior compartment of the leg was left intact. Briefly, anesthesia was induced with a subcutaneous injection of ketamine/xylazine cocktail (35 and 5 mg/kg respectively) and maintained with 2% isofluorane (2 L/min). Heart rate, blood oxygen saturation (PhysioSuite, Kent Scientific Corp., Torrington, Connecticut) and respiratory rate were monitored during all tests. Physiological temperature and moisture were maintained throughout the experiment.

The TA and peroneal nerve were surgically exposed, and the hind limb immobilized in a custom made jig. The distal TA tendon was transected, released from the retinaculum, and clamped at the muscle-tendon junction to a servomotor (Aurora Scientific Inc., Canada). Force generation axes of the TA and servomotor were carefully aligned. A cuff electrode (Model S48, Grass Instruments, Quincy, MA) provided direct stimulation to the peroneal nerve. Supramaximal excitation voltage and optimum fiber length were measured experimentally for each TA using twitch contractions. Once these baseline conditions were established, isometric force from tetanic contractions was measured twice before and twice after probe insertion (5 V typical, 0.3 ms pulse width,

100 Hz frequency, 640 ms duration) with two-minute rest between contractions. Rabbits were then euthanized with 120 mg/kg pentobarbital injected into the marginal ear vein.

5.2.2 Isometric force measurements

To quantify structural and functional damage associated with our probe, isometric force of rabbit tibialis anterior (TA) muscles (N = 7 muscles, 4 rabbits) was measured before and after insertion of a prototype intramuscular lensed optical probe (OZ Optics, Canada). In this group of experiments, the extensor digitorum longus tendon was cut to limit lateral force transmission. In later experiments, the tendon was left intact, but the foot was clamped down. This served to allow ground the force production of the extensor digitorum longus.

Probe insertion was performed with the following procedure. An optical probe was threaded into but not extended past the tip of a 22 gauge hypodermic needle; the needle was inserted approximately 1 cm into the mid-belly of the TA, parallel to muscle fibers. While holding the optical probe in place, the hypodermic needle was removed from the muscle before stimulating contractions. In three animals, the procedure was repeated for the contralateral limb. After contractions, the probe was removed and inspected for damage. No probes were damaged using this protocol.

5.2.3 Histology

To determine the structural damage induced by probe insertion, following sacrifice, TA muscles were excised and pinned to cork at resting length. An optical probe was re-inserted into the muscle distal to the first insertion point, but otherwise following the same procedure. Then, muscle and probe were flash frozen. Probes were carefully

removed just before sectioning, though three probes broke during removal and corresponding muscles were not counted in further analysis.

Cross-sections were taken from flash frozen muscles (N = 4) at 70 μm thickness using a cryostat (Microm HM500, Waldorf, Germany). This thickness was found to best maintain the integrity of probe induced holes, although it was thicker than the optimal value needed for muscle morphology. Sections were stained with hematoxylin and eosin (H&E) for visualization and imaged with a light microscope (Model DM6000, Leica Microsystems Inc., Buffalo Grove, Illinois). Area fraction of probe-induced damage was calculated using ImageJ [6].

5.2.4 Muscle function after intramuscular insertion of optical probes

Future RRS applications may require intramuscular insertion of optical probes. To access the amount of muscular damage induced by probe insertion, we measured maximal isometric contractile force in rabbit TA muscles before and after prototype lensed optical probe insertion (Figs. 4.4 *A* and *B*). There was almost no change in contractile force with probe insertion (see sample records in Fig. 4.4*A*). Further, averaged pre-insertion and averaged post-insertion forces were not significantly different (Fig. 4.4*B*, paired t-test, P = 0.213). Power analysis indicated an 80% power to detect a 5% force change given the experimental variability.

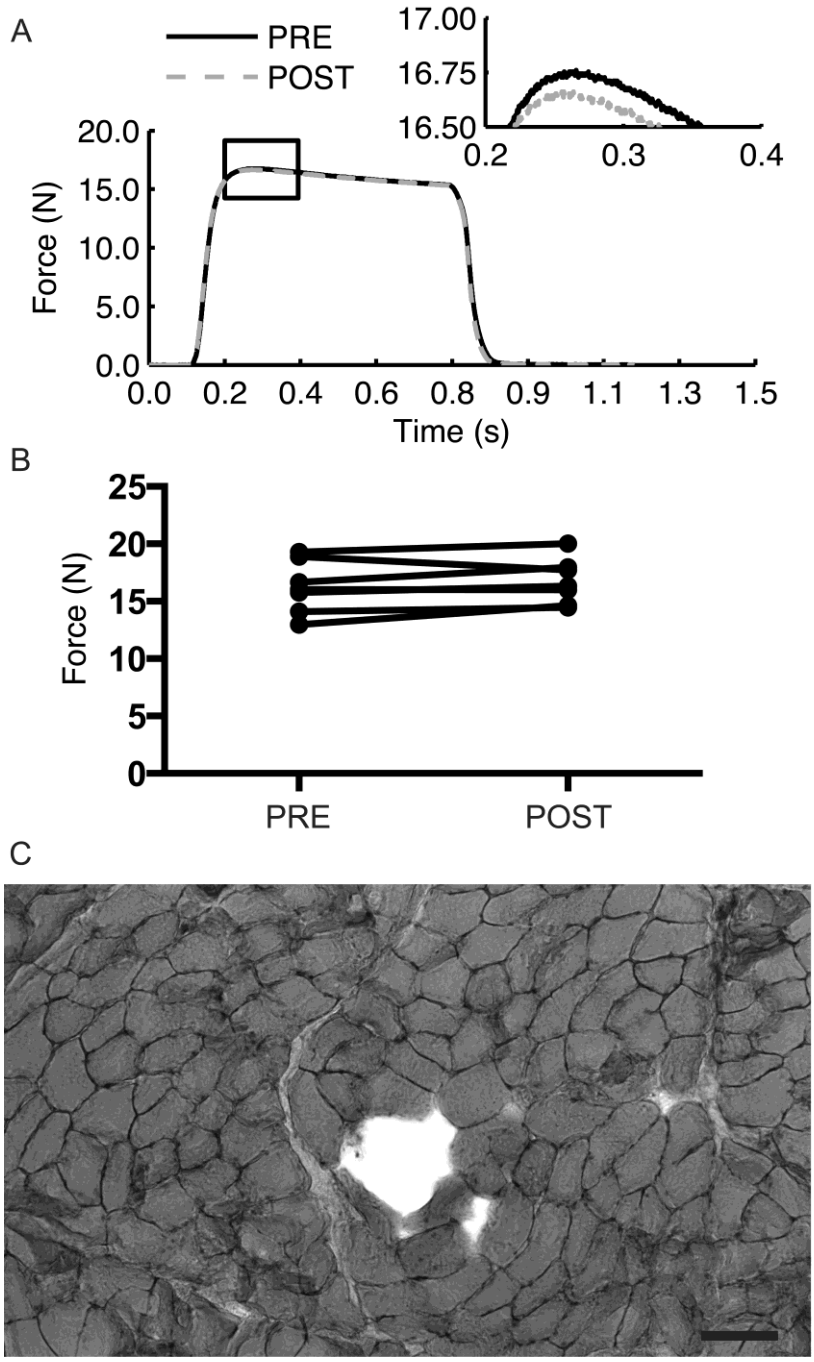

Figure 5.1: Insertion of an optical probe has almost no effect on structure or function. (*A*) Representative isometric contractile record of a rabbit TA pre- and post-insertion of an optical probe. Inset shows the force record enlarged at the plateau. (*B*) Paired t-test shows that isometric muscle function is not significantly different after probe insertion (P = 0.213). (*C*) Representative 70 µm thick cross-section of a rabbit TA muscle stained with hematoxylin and eosin shows area of probe insertion. Average damaged area fraction was 0.078%. Scale bar represents 0.1 µm.

To assess the structural damage caused by probe insertion, we examined corresponding cross-sections of rabbit TA muscles stained with H&E (Fig. 4.4*C*). Damaged muscle area fraction, calculated as area of damage divided by muscle cross-sectional area, associated with probe insertion was found to be 0.078%. Taken together, these data suggest that optical probe insertion into muscle has almost no effect on structure or function.

5.3 Minimally invasive sarcomere length measurement with nanometer resolution across millimeters of tissue

With the goal of simultaneously measuring along millimeters of muscle tissue with kHz sampling rate, nm resolution, compatibility with gross movement, and minimal tissue damage, we developed a new technique termed resonant reflection spectroscopy (RRS) [7]. We previously provided proof of concept and measurement validation *in vitro* [7]. Here, we report RRS feasibility for functional sarcomere length measurement *in vivo*. We achieved sample sizes up to 4,200 sarcomeres sampled at 9.85 kHz using a 250 μm diameter fiber optic probe during passive stretch, twitches, and tetanic contractions.

RRS is a low-power technique that relates transmission and reflection of light within a periodic material to its underlying structure [7, 8]. Skeletal muscle sarcomeres provide a unique periodic structure that interacts strongly with laser light. In traditional laser diffraction, a single wavelength laser illuminates sarcomeres perpendicular to their long axis, and the transmitted diffraction pattern is used to calculate sarcomere length[9–11]. RRS differs from traditional laser diffraction by rotating the illumination and collection geometry to be parallel with the sarcomere long axis. This enables illumination

and collection of the necessary data using a single small fiber optic probe. This trade-off of reducing spatial complexity is a dramatically increased optical wavelength range that is not available to most laser sources [7]. To satisfy the wavelength requirement, we employ custom technology developed for optical communication [7, 12]. However, for the purposes of providing proof of feasibility, here we use a commercially available source along with a corresponding reduction in measurable sarcomere length range.

5.3.1 Optical system

A swept wavelength laser (ESS, Exalos AG) continuously sweeps from 1483 to 1598 nm wavelength. Laser energy is split using a fiber optic coupler between a measurement and reference arm. In the measurement arm, laser energy is delivered to muscle through an optical circulator through a 250 μm lensed fiber optic probe (OZ Optics) inserted directly into the muscle belly. Care is taken to align fiber optic and muscle fiber long axis. The same optical probe collects muscle reflections that are then combined with the reference arm using a second optical coupler. The reference arm contained a polarization controller and a tunable delay line for controlling focal depth. Combined reference and measurement arms were split with a polarization beam splitter to minimize polarization-induced fringe fading. Inteferograms at the output of the polarization beam splitter were measured by a pair of amplified photodetectors (PDF10C Thorlabs) and digitized (5444B Pico Technology). Custom Labview software controlled the system. Resonant reflection spectra are encoded in inteferograms and used to calculate sarcomere length with nm resolution in 30 μm spaced distance bins and 1 ms time resolution.

5.3.2 Muscle physiology

Rabbits were placed under anesthesia using previously described methods with approval from the Institutional Animal Care and Use Committee [4]. Briefly, tibialis anterior muscle and peroneal nerve were surgically exposed. MTU force and length were measured by clamping the distal tendon 1 cm from the muscle tendon junction into a force transducer and the hind limb was immobilized. A cuff electrode stimulated the peroneal nerve during active trials. After experimentation, rabbits were euthanized with 120 mg/kg pentobarbital injected into the marginal ear vein.

5.3.3 Signal processing

Custom Matlab software was written to perform data analysis. A digital trigger was used to register muscle force and length measurements with optical signals. DC signal was subtracted from the data, and spectra were linearized to equal spaced optical frequency points using the swept laser's k-clock. Data were averaged over 1 ms to improve signal-to-noise ratio. Resonant peaks in OFDI spectra from within the muscle were filtered in the Fourier domain. Filtered resonant peaks were Fourier transformed back to resonant spectra using discrete Fourier transform. Sarcomere length was calculated both by Bragg's law and correlations to a simulated resonant spectra lookup table, but there was no difference between the two estimates. Data reported here are from calculations by Bragg's law.

5.3.4 Results

Histological examination of tissue shows that sarcomere lengths adjacent to probe insertion were within 5% coefficient of variation, which is typical to other skeletal

muscle [13]. However, variable contact at the surface of the probe tip caused by motion or wound response may change baseline reflection spectra thus invalidating sarcomere lengths measured. To address this concern, we implemented optical frequency domain interferometry (OFDI) to encode reflection spectra inside interferograms of different frequency [14]. OFDI yields depth resolution that enables separation of reflections from the probe surface from reflections within the muscle tissue. Importantly, it enables profiling sarcomere length along many millimeters of muscle.

Our proof of feasibility (Fig. 1), which combines OFDI and RRS, enabled sarcomere length measurement during dynamic movement and activity. We used a commercially available source with relatively limited optical wavelength range that creates two limitations to RRS: First, sarcomere length degeneracy could result if we were uncertain of approximate sarcomere length. Second, data can only be measured within specific sarcomere length windows. These limitations can only result in false negatives, and therefore they do not affect the interpretation or proof of feasibility presented here. To demonstrate feasibility, we measured sarcomere length during dynamic movements with trials consisting of passive stenches, twitches, and isometric tetanic contractions. An example of each trial is included here.

Passive strains consisted of linear strain to the MTU, hold, and linear shortening. Sarcomere length was measured throughout the trial (Fig. 2). Several false negatives, where no sarcomere length is measured, occurred. Sarcomere length change during each phase of the passive strain trial showed the expected non-linear behavior associated with viscoelastic biological tissue [15].

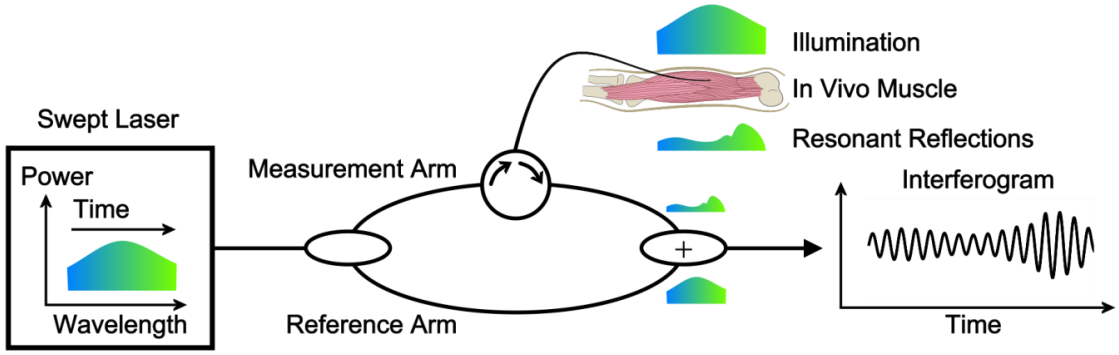

Figure 5.2: Minimally invasive sarcomere length profiler. A swept wavelength laser source continuously sweeps across wavelength. Laser energy is split between a measurement and reference arm. In the measurement arm, laser energy is delivered to muscle through an inserted fiber optic probe with 250 µm diameter. The same optical probe collects muscle reflections that are then combined with the reference arm and sent to a detector. Resonant reflection spectra are encoded into inteferograms and used to calculate sarcomere length with nm resolution in 30 µm spaced distance bins and 1 ms time resolution.

During passive strain, sarcomere length change was concave and non-linear due to series connective tissue viscoelasticity. High viscoelastic force within the series tendon forces all strain to be taken by sarcomeres, which results in a greater sarcomere strain than tendon strain. As strain continues, series tendon absorbs strain and relative sarcomere strain rate decreases. An interesting dynamic occurs between muscle elasticity and series tendon viscoelastic components during hold after passive strain. Sarcomere length shortens during the hold phase of the MTU, which means muscle elasticity allows tendon creep. Sarcomere strain is convex during passive shortening of the MTU for the opposite reason as described above. These *in vivo* data represent the first dynamic sarcomere lengths measured from intact mammalian skeletal muscles with nanometer length resolution maintained across millimeters of muscle tissue. Additionally, RRS spectra contain a wealth of information about the protein ultrastructure (Fig 2. Insets).

Peak wavelength is used here to calculate sarcomere length. Additionally, measuring filament length and the complete reconstruction of sarcomere proteins in 3D are theoretically possible using the full reflection profile and phase response [16]. Protein filament length and their arrangement are critical to understating muscular dystrophy pathology and its progression [17].

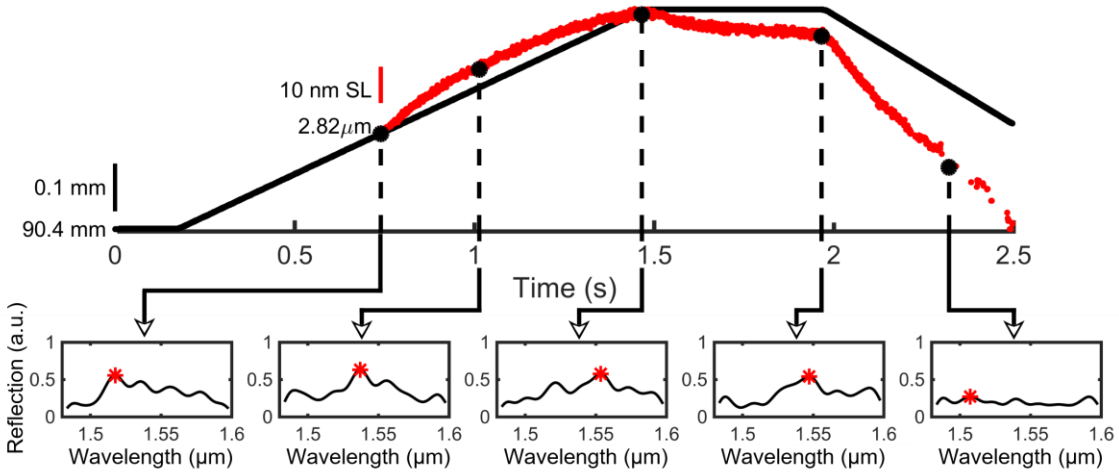

Figure 5.3: Sarcomere length as a function of passive strain of the MTU (black). Top plot shows sarcomere length as the MTU was linearly strained, held, and then returned. Sarcomere length change (red) show clear nonlinearities during each phase. Insets show sample resonate reflection spectra that provide sarcomere length estimates.

Second, a twitch is the fundamental quantum of force production in striated muscle [18]. Direct measurement of a sarcomere response to electrical impulses provides the exciting opportunity to probe the relationship between electric drive and muscular response. To access the feasibility of RRS to measure sarcomere length during isometric twitch, we excited the peroneal nerve with a cuff electrode.

Sarcomere shortening occurred simultaneously with activation and force was transmitted directly to the force transducer (Fig. 3). Sarcomere length shortened linearly and reached the plateau over 30.4 ms. After 38.7 ms sarcomeres lengthened non-linearly as calcium was returned to the sarcoplasmic reticulum. Across all twitches, we found no truly isometric contractions reflecting sarcomere shortening at the expense of tendon lengthening. False negatives only occurred during the activation phase, which is consistent with previous studies that suggest sarcomeres are disordered upon activation [19].

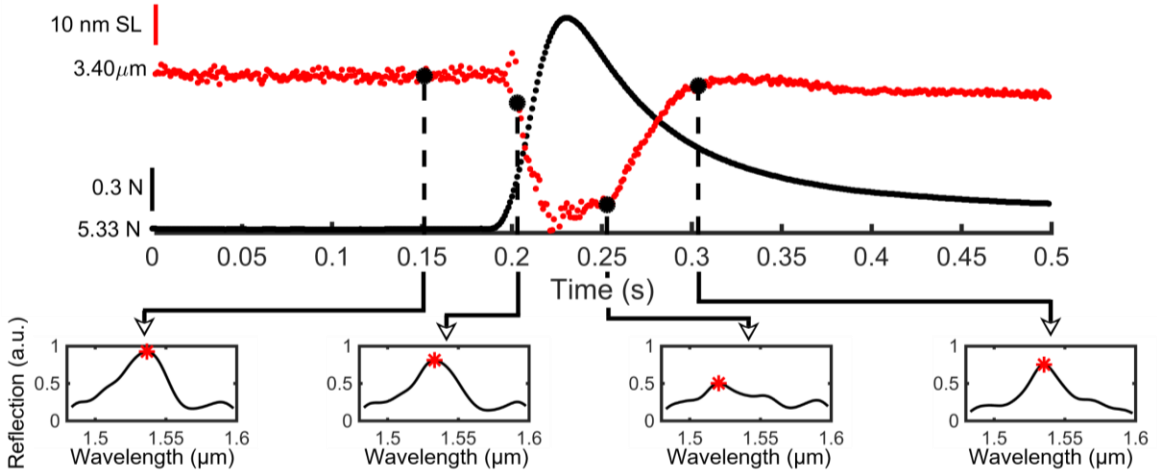

Figure 5.4: Sample data from an isometric twitch. Top plot shows sarcomere length (red) and force data (blue). Sarcomere length changes are remarkably linear during force production. Insets show sample resonate reflection spectra that provide sarcomere length estimates.

Third, tetanic contractions, the most common type of muscle contraction, revealed *in vivo* sarcomere length shortening as a result of tendon series viscoelasticity (Fig. 4). Although the MTU was kept at a constant length, sarcomeres shorten well past the initial rise in force, due to series connective tissue compliance [20]. On the descending limb of

the length tension curve, as is the case in this example trial, sarcomeres become stronger as they shorten. Stronger sarcomeres produce more stress and the tendon lengthens further. This process repeats until steady state was reached after 330 ms. False negatives predominately occurred in two regions. As with the twitch trial, sarcomeres become disordered during the onset of activation. Sarcomere length also dramatically changes when activation ends, which we have demonstrated previously *in vitro* [21]. Improved SNR, optical bandwidth, and optical probe design would eliminate false negatives.

The ability to separate muscle force production from neuronal drive is critical in diagnosing deficits in strength or movement in patients with muscle dystrophy and cerebral palsy. We believe that the technique described here will enable routine measurement of muscle protein structure to revolutionize our diagnosis and treatment these diseases.

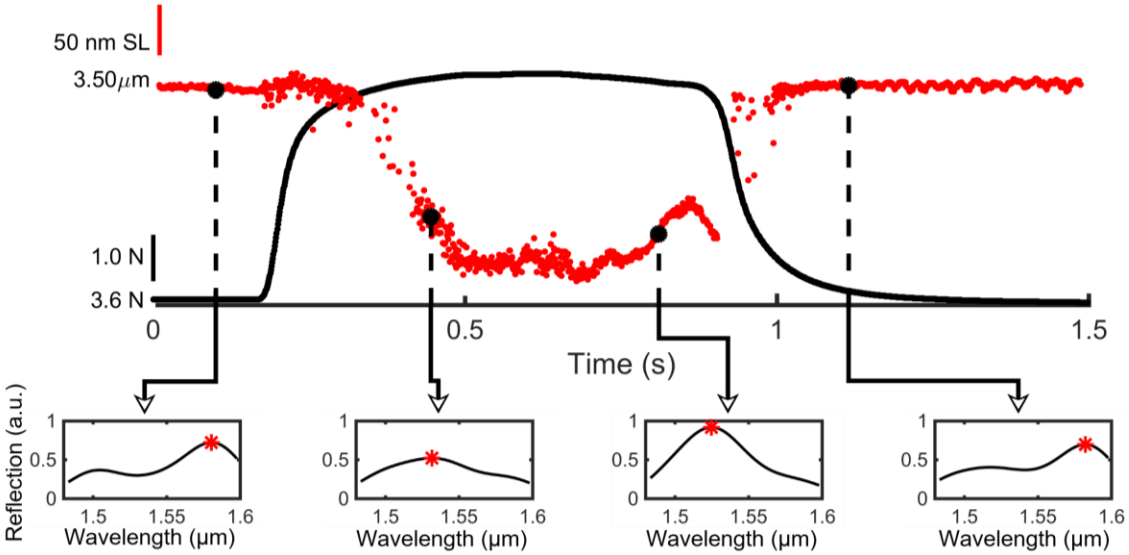

Figure 5.5: Sample trial of sarcomere length during an isometric tetanic contraction. Top plot shows sarcomere length (red) and MTU force (blue) as a function of time. Sarcomeres shorten linearly for an extended period of time due to series compliance. Insets show sample resonate reflection spectra that provide sarcomere length estimates.

5.6 Acknowledgements

Chapter 5 is a combination of sections from two papers. Several sections are nearly identical to sections of a peer reviewed article entitled “Resonant reflection spectroscopy of biomolecular arrays in muscle” by Young KW, Radic S, Myslivets E, O’Connor SM, and Lieber RL. Other sections are nearly identical to a manuscript entitled “In Vivo Minimally-Invasive Molecular Sensing across Millimeters of Muscle Tissue during Movement” by Young KW, Kuo P.-P., O’Connor SM, Radic S, and Lieber RL, that is in preparation for submission to a peer reviewed article.

5.7 References

1. Chung K, Wallace J, Kim S-Y, Kalyanasundaram S, Andalman AS, Davidson TJ, Mirzabekov JJ, Zalocusky KA, Mattis J, Denisin AK, Pak S, Bernstein H, Ramakrishnan C, Grosenick L, Gradinaru V, Deisseroth K: **Structural and molecular interrogation of intact biological systems.** *Nature* 2013, **497**:332–7.

2. Airan RD, Thompson KR, Fenno LE, Bernstein H, Deisseroth K: **Temporally precise in vivo control of intracellular signalling**. *Nature* 2009, **458**:1025–1029.

3. Winters T, Takahashi M, Lieber R, Ward S: **Whole muscle length-tension relationships are accurately modeled as scaled sarcomeres in rabbit hindlimb muscles**. *J Biomech* 2011, **44**:109–115.

4. Lieber RL, Woodburn TM, Fridén J: **Muscle damage induced by eccentric contractions of 25% strain.** *J Appl Physiol* 1991, **70**:2498–2507.

5. Davis J, Kaufman KR, Lieber RL: **Correlation between active and passive isometric force and intramuscular pressure in the isolated rabbit tibialis anterior muscle**. *J Biomech* 2003, **36**:505–512.

6. Rasband WS: **ImageJ**. *U.S. National Institutes of Health, Bethesda, Maryland, USA* .

7. Young KW, Radic S, Myslivets E, O'Connor SM, Lieber RL: **Resonant reflection spectroscopy of biomolecular arrays in muscle**. *Biophys J* 2014, **107**:2352–2360.

8. Erdogan T: **Fiber grating spectra**. *J Light Technol* 1997, **15**:1277–1294.

9. Cleworth D, Edman K: **Changes in sarcomere length during isometric tension development in frog skeletal muscle**. *J Physiol* 1972, **227**:1–17.

10. Yeh Y, Baskin RJ, Lieber RL, Roos KP: **Theory of light diffraction by single skeletal muscle fibers.** *Biophys J* 1980, **29**:509–22.

11. Sidick E, Baskin RJ, Yeh Y, Knoesen a: **Rigorous analysis of light diffraction ellipsometry by striated muscle fibers.** *Biophys J* 1994, **66**:2051–61.

12. Kuo BP-P, Radic S: **Highly nonlinear fiber with dispersive characteristic invariant to fabrication fluctuations**. *Opt Express* 2012, **20**:7716.

13. O'Connor SM, Cheng EJ, Ward SR, Lieber RL: **Sarcomere Length Variation of Whole Skeletal Muscle**. In *ORS Annual Meeting*; 2016.

14. Soller B, Gifford D, Wolfe M, Froggatt M: **High resolution optical frequency domain reflectometry for characterization of components and assemblies**. *Opt Express* 2005, **13**:1735–1740.

15. Fung Y: *Biomechanics: Mechanical Properties of Living Tissues*. Springer Science & Business Media; 2013.

16. Rosenthal A, Horowitz M: **Inverse scattering algorithm for reconstructing strongly reflecting fiber Bragg gratings**. *Quantum Electron IEEE J* 2003, **39**:1018–1026.

17. Gehrig SM, van der Poel C, Sayer TA, Schertzer JD, Henstridge DC, Church JE, Lamon S, Russell AP, Davies KE, Febbraio MA, Lynch GS: **Hsp72 preserves muscle function and slows progression of severe muscular dystrophy**. *Nature* 2012, **484**:394–398.

18. Hoffer AJA, Donovan MJO, Pratt CA, Loeb GE: **Discharge Patterns of Hindlimb Motorneurons during Nomral Cat Locomotion**. *Science (80-)* 1981, **213**:466–468.

19. Yeh Y, Pinsky BG: **Optical polarization properties of the diffraction spectra from single fibers of skeletal muscle.** *Biophys J* 1983, **42**:83–90.

20. Edman K, Reggiani C: **Redistribution of sarcomere length during isometric contraction of frog muscle fibres and its relation to tension creep**. *J Physiol* 1984, **351**:169–198.

21. Patel TJ, Das R, Friden J, Lutz GJ, Lieber RL: **Sarcomere strain and heterogeneity correlate with injury to frog skeletal mucsle fiber bundles**. *J Appl Physiol* 2004, **97**:1803–1813.

Chapter 6 Improving Swept Source Fiber Optic Parametric Oscillators

6.1 Introduction

Wavelength swept sources are used in widespread fields such as medical imaging and spectroscopic sensing [1–3]. Optical bandwidth and wavelength sweep rate are application specific, but generally broader and faster sweeps are desireable to maximize information and time resolution. These metrics are especially important in emerging biological sensing technology. For example, we recently showed proof of feasibility for a protein-scale sensing technique termed resonant reflection spectroscopy (RRS) to measure skeletal muscle kenetics in vivo [4]. This demonstration leveraged swept laser sources to perform optical frequency domain interferometry (OFDI) in conjuction to RRS for depth resolved measurements of muscle function [1, 2]. However, available commercial swept sources provide only a fraction of the ideal bandwidth to perform RRS, and so the system was limited to specific muscle lengths [4]. Bandwidth in commercial swept wavelength sources are limited to the optical gain available from electron transitions in the medium used, so additional methods are necessary to extend the naitive bandwidth of a swept source. Additionaly, conventional swept sources require a two-step process to create a wavelength sweep. First, full bandwidth of the gain medium is engaged. Second, a passive filter restricts circulation in the laser cavity to narrow wavelength band [5]. In swept operation, the wavelength filter is mechanically modulated to create the wavelength sweep, and speed is limited by the mechanical speed of filter tuning.

One potential solution to increase bandwidth while maintaining fast speed is through using a swept-pump fiber optical parametric oscillator (FOPO) system.

Previously, we have shown simultaneous wavelength-swept generation across 329 nm optical wavelength [6]. Current FOPOs, however, are too slow to be used during muscle activity and motion. Here we develop several design rules to improve FOPO systems. By variable tuning of power and repetition rate we increase sweep speed to 14 kHz and increase optical bandwidth to a total of 422 nm. These design rules can be used to design future systems, such as an engine in a new RRS system to measure a much more general set of muscles.

6.2. System architecture

6.2.1 Operating principles

FOPOs use a swept source as the input (pump) to a precisely engineered optical cavity. The FOPO cavity contains a narrow band fiber optic parametric amplifier (FOPA) that generates Stokes and anti-Stokes beams from the seed wavelength. Resulting Stokes and anti-Stokes beams can be cast to far wavelengths that are not available from conventional laser sources. As the seed wavelength is swept, the Stokes and anti-Stokes beams are swept by a larger factor that is controlled by the parametric amplification process, and total bandwidth is dramatically increased (Fig. 1). Efficient energy transfer from pump to Stokes and anti-Stokes beams is achieved by circulating the anti-Stokes inside a lasing cavity. Theoretical considerations for the FOPA used in the FOPO are discussed in detail elsewhere [6]. Here, we investigate practical design rules for optimizing and designing these systems.

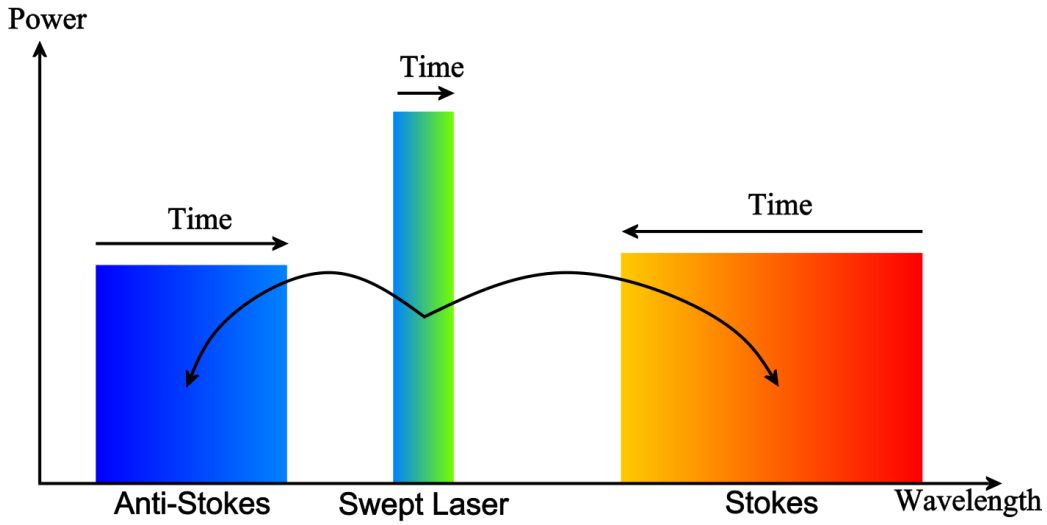

Figure 6.1: Swept source operation within FOPO cavity.

6.2.2 Experimental system

A new FOPO system was built to achieve faster repetition rate and increased bandwidth (Fig. 2). Insight Photonic Solutions' akinetic swept laser was chosen as the seed swept source. We found the programmable bandwidth and sweep speed critical to optimization. This pump also allowed static and dynamic operation of the FOPO, which allowed us to optimize between dynamic and static cases with the same exact system. During static operation, wavelength was stepped from 1527 nm to 1565 nm in 1 nm increments to explore maximal achievable bandwidth. During dynamic operation, pump wavelength was swept from 1536 to 1564 nm at 14 kHz sweep rate.

The Insight akinetic laser output at 15 dBm was sent to a Mach-Zehnder modulator (MZM) to generate optical pulses. Pulse repetition rate was controlled by one of three clocks; clock choice and rational are discussed in Section 3.3. Duty cycle was controlled by a tunable pulse generator (Alnair EPG-210B). During dynamic operation, the clock driving pulse optical pulse creation of the MZM was linearly swept from

10.429 to 10.432 MHz repetition rate in sync with the swept laser to accomodate wavelength differences to index of refraction within the laser cavity. Optical pulses at the output of the MZM were amplified in two stages by erbium-doped fiber amplifiers (EDFA1 and EDFA2). Power to EDFA2 was variable during dynamic operation of the FOPO; more details and rational are discussed in Section 3.2. High power pump pulses were sent to the FOPO cavity. FOPA parametric gain medium was a highly non-linear fiber (HNLF) with zero-dispersion wavelength (ZDW) of 1567.3 nm[7]. FOPA output was monitored by a 1% tap using an optical coupler (OC). Two wavelength division multiplexes (WDM1 and WDM2) served to circulate only anti-Stokes (lasing) waves in the FOPO cavity. Isolated short-wave infrared (SWIR) and near infrared (NIR) beams could be obtained at WDM2 and 30% of the intra-cavity OC, respectively.

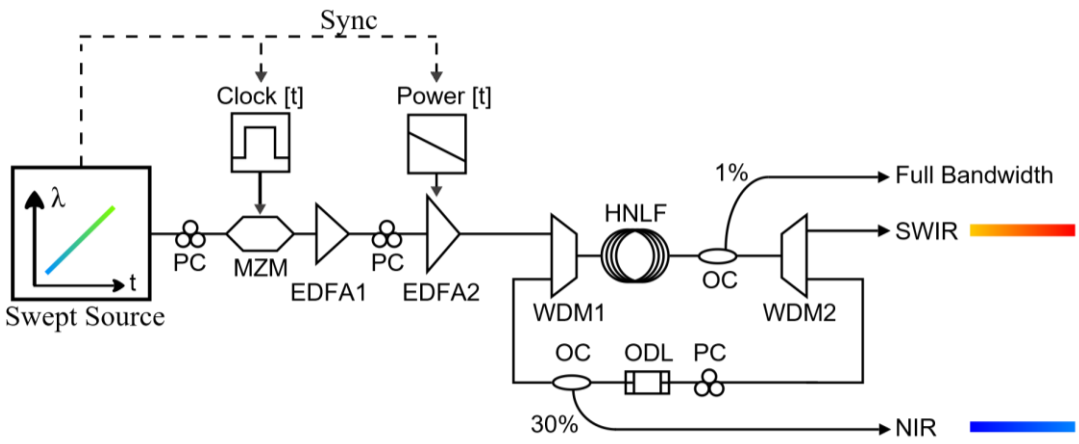

Figure 6.2: FOPO system architecture.

6.3. Static wavelength operation

6.3.1 Bandwidth limits

Bandwidth limits of the FOPO were investigated under static operation of the pump (Fig. 3). Wavelength spectra were collected by an optical spectra analyzer at the

output of the 1% FOPA tap (Yokogawa, Japan). Pump wavelength was stepped from 1527 nm to 1565 nm in 1 nm increments. Resulting spectra show a remarkable 1800% increase in output bandwidth. Energy is very efficiently transferred to the lasing anti-stokes wave. In most cases, anti-stokes power reached within 3 dB of pump power. Energy transfer to stokes waves is less efficient at ~15 dB down from pump power for most pump wavelengths. Repetition rate was adjusted for each pump wavelength. Power level was optimized for the shortest pump wavelengths and was kept constant for all trials. Constant power level has a profound effect on FOPO performance and is discussed in the next section.

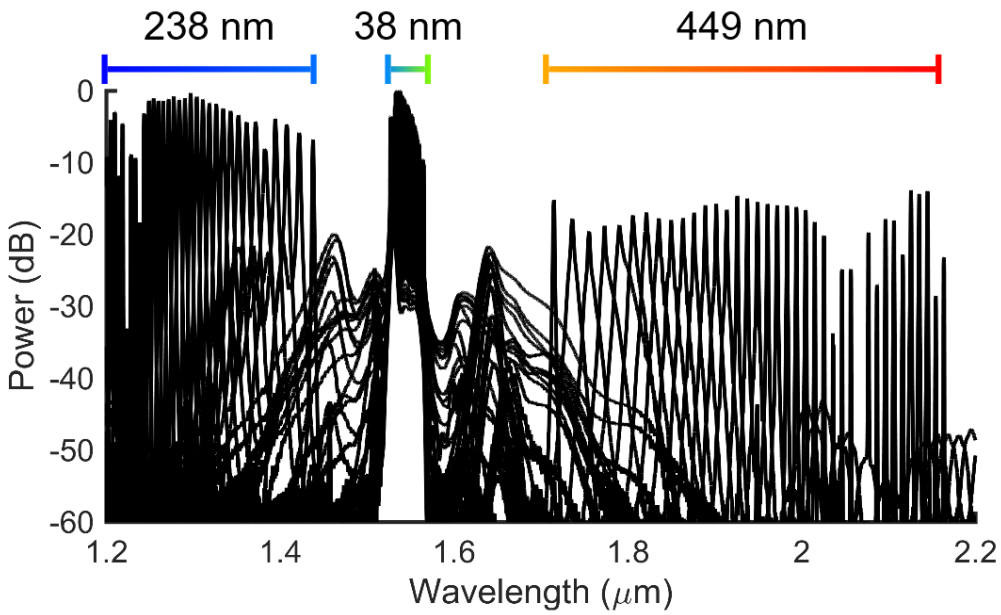

Figure 6.3: FOPO bandwidth limits during static operation. Each trace is associated with a different pump wavelength.

6.3.2 Booster drive optimization

As can be seen in Fig. 3, the necessary power level at the short wavelength side is over-amplified for the long wavelength side. This is evidenced by the dramatic widening

of beam width for the over powered NIR and SWIR waves [6]. This occurs despite the natural occurrence of lower pump amplification at the longer wavelength beams for the EDFAs used, as evidenced by to drop-off in peak power of the pump at short wavelengths compared to longer wavelengths. To combat this feature during dynamic operation, we swept EDFA2 drive voltage in sync with the pump sweep (Fig. 4). Internal capacitance of the EDFA2 resulted in a delayed impulse response. We found the voltage drive profile shown in Fig. 4 to best optimize the balance between power necessary for short wavelengths with over-powering the long wavelength side of the pump.

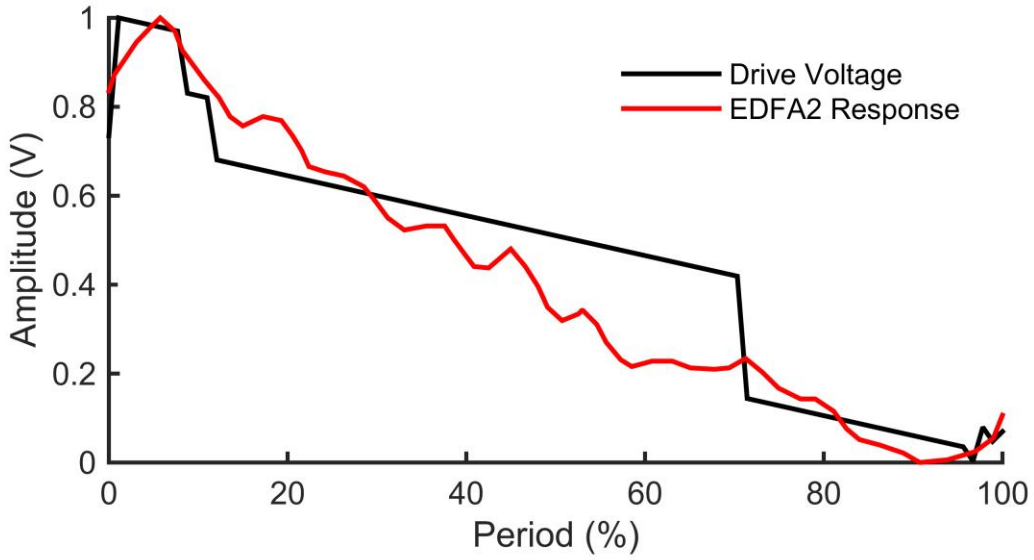

Figure 6.4: System optimization. (A) Clock stability dramatically affects power stability. (B) Optimium drive voltage to the system booster and booster power response during swept optimization.

6.3.3 Repetition rate optimization

Fundamental cavity frequency was measured as approximately 880 kHz. Practicle application of FOPO to spectroscopy requires sub-nanometer wavelength resolution, so we used approximately 10.43 MHz repetition rate to create pulses at sub-nanometer

wavelength spacing. However, faster repetition rates require more narrow pulses to maintain a short duty cycle to achieve sufficient peak power for efficient parametric amplification. We found that MHz-scale repetition rate required approximately 500 ps duration pulses. Sub-nanosecond pulses significantly increase lasing loss due to walk-off between circulating pulses, particularly for dynamic operation where wavelength differences in index of refraction contribute to cavity de-tuning. To address this caveat, Optimal repetition rate of pump pulses was measured during static operation (Fig. 5). We found a highly non-linear relationship between optimal repetition rate and wavelength.

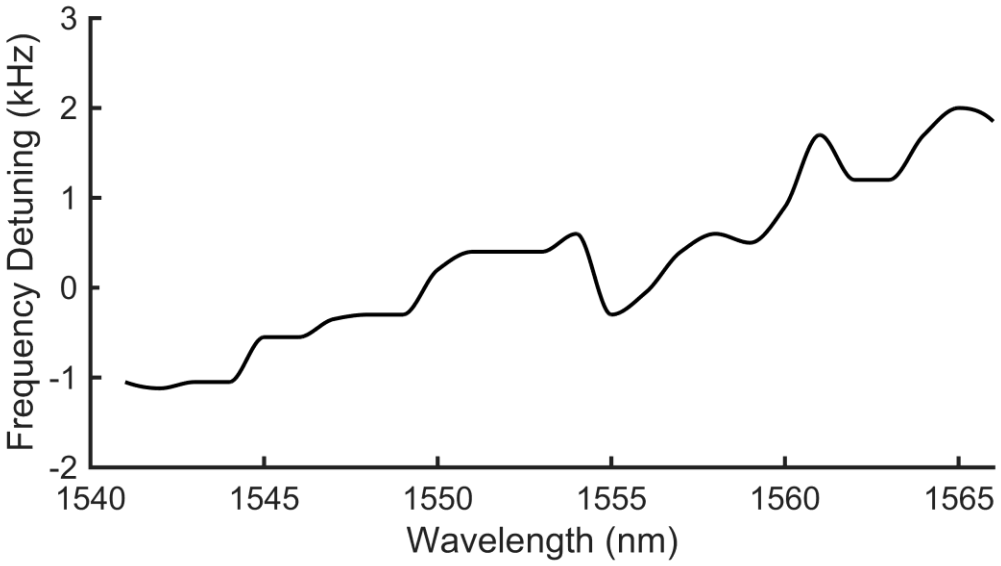

Figure 6.5: Optimal frequency detuning from 10.43 MHz repeitition rate as a function of wavelength in static operation.

Unfortunately, high quality clocks that output non-linear frequency sweeps are not readily available. We tested three clocks in static operation of the FOPO and found that clock stability to have a much more significant effect that optimal repetition rate (Fig. 6). Clocks tested were VCO, AWG1 and AWG2. To best combine cavity frequency as a

function of wavelength and clock stability, we used a clock with very low jitter that was able to produce linear frequency sweeps in sync with the pump sweep.

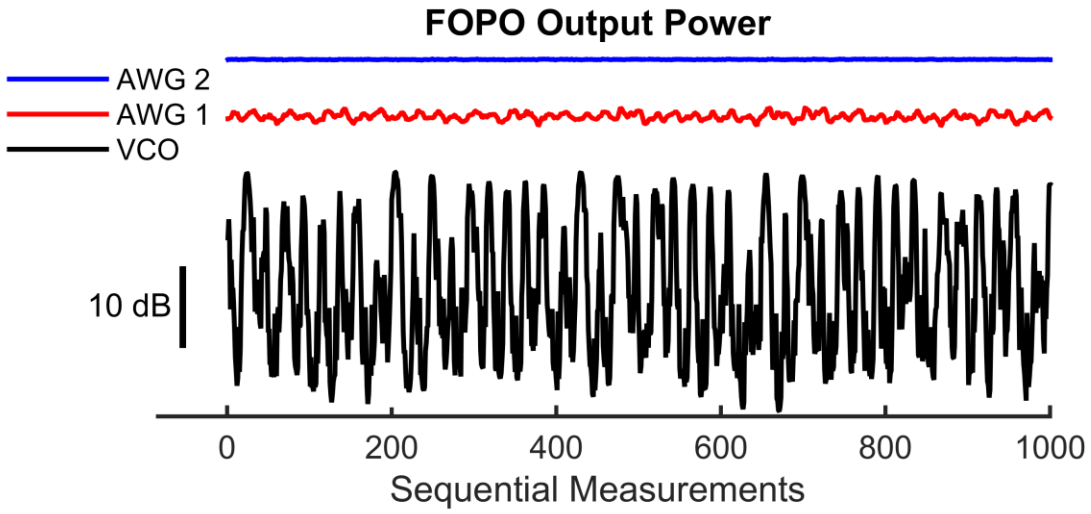

Figure 6.6: System optimization. (A) Clock stability dramatically affects power stability. (B) Optimium drive voltage to the system booster and booster power response during swept optimization.

6.4 Dynamic wavelength operation

By utilizing the design rules discussed above, we achieved 14 kHz sweep rate with total bandwidth equal 422 nm in dynamic operation of the FOPO (Fig. 7). The full output spectrum of the wavelength-swept FOPO at the 1% tap after the HNFL shows significant Raman gain between pump and Stokes bands. This unintended gain results from lasing deficiencies at the edges of the wavelength sweep. Further improvements through non-linear optimization of repetition rate and improved passive filtering in the lasing cavity are expected to eliminate Raman gain and reach greater than 725 nm bandwidth shown in static operation.

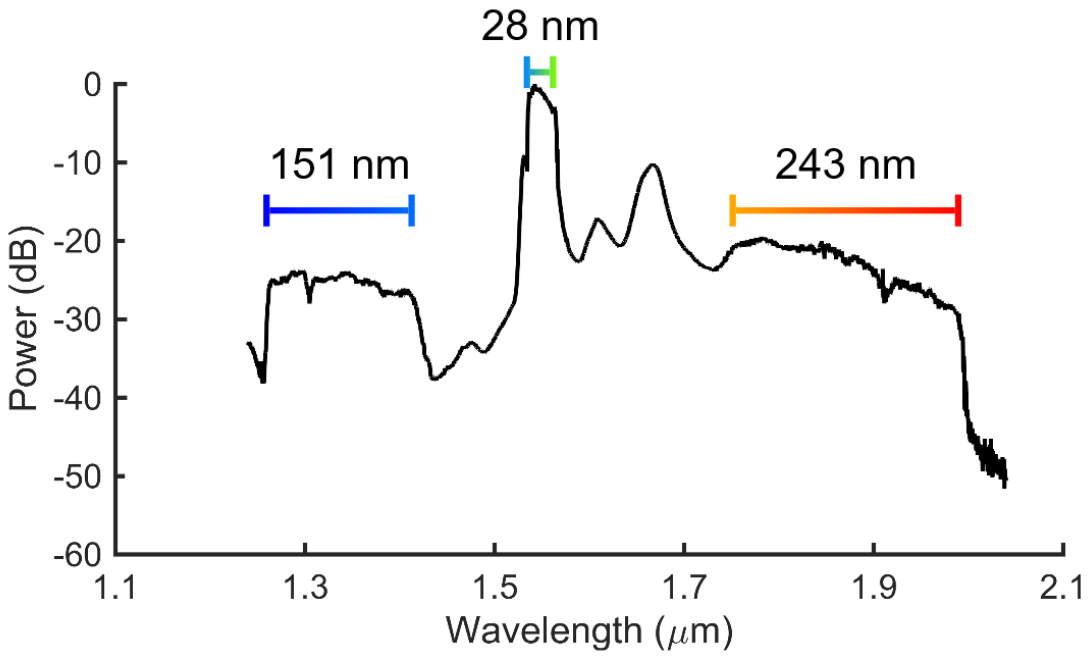

Figure 6.7: FOPO performance at 14 kHz repetition rate.

6.5. Conclusion

We report conception and implementation of new design rules for FOPO systems. Using a sweeping tunable pump across 28 nm, our new system achieves a record breaking 422 nm combined bandwidth at 14 kHz repetition rate, which equates to 3400000 nm/s sweep speed in the Stokes band. This engine can be used in many techniques where bandwidth and sweep speed are key parameters, such as resonant reflection spectroscopy.

6.6 Acknowledgements

Chapter 6 is nearly identical to a manuscript entitled “Swept-Pump Fiber Optical Parametric Oscillator with 422 nm Bandwidth and 14 kHz Scan Rate Achieved with Variable Control” by Young KW, Kuo P.-P., Lieber RL, and Radic S, that is in

preparation for submission to a peer reviewed article. This work was funded by the Department of Veteran's Affairs Grant A9028R, NIH Grant R24 HD050837, and private donation by the Elden Foundation.

6.7 References

1. Chinn SR, Swanson EA, Fujimoto JG: **Optical coherence tomography using a frequency-tunable optical source**. *Opt Lett* 1997, **22**:340–342.

2. Soller B, Gifford D, Wolfe M, Froggatt M: **High resolution optical frequency domain reflectometry for characterization of components and assemblies**. *Opt Express* 2005, **13**:1735–1740.

3. Eckhoff WC, Putnam RS, Wang S, Curl RF, Tittel FK: **A continuously tunable long-wavelength cw IR source for high-resolution spectroscopy and trace-gas detection.** *Appl Phys B* 1996, 63:437–441.

4. Young KW, Radic S, Myslivets E, O'Connor SM, Lieber RL: **Resonant reflection spectroscopy of biomolecular arrays in muscle**. *Biophys J* 2014, **107**:2352–2360.

5. Wysocki PF, Digonnet MJF, Kim BY: **Broad-spectrum, wavelength-swept, erbium-doped fiber laser at 1.55 μm**. *Opt Lett* 1990, **15**:879–881.

6. Kuo BP-P, Alic N, Wysocki PF, Radic S: **Simultaneous wavelength-swept generation in NIR and SWIR bands over combined 329 nm band using swept-pump fiber optical parametric oscillator**. *J Light Technol* 2011, **29**:410–416.

7. Kuo BP-P, Radic S: **Highly nonlinear fiber with dispersive characteristic invariant to fabrication fluctuations**. *Opt Express* 2012, **20**:7716–7725.

Chapter 7 Conclusion

7.1 Dissertation Summary and Significance

Significant progress in a field of study relies on the collection of high quality data. In skeletal muscle physiology, the greatest hindrance to progress is the inability to measure muscle protein structure during realistic movement. The goal of this thesis was to leverage several decades of technological development in the field of fiber optic communication that was so far un-tapped in the field of muscle physiology.

The first contribution of this thesis in Chapter 2 was increasing the sensitivity of using laser diffraction to measure skeletal muscle sarcomere length in muscle fibrosis. Muscle fibrosis is associated with many diseases and includes a significant increase in muscle collagen content. Collagen is highly scattering and typically disables the use of laser diffraction to measure sarcomere length by burying the needed diffraction signal in scattered noise. Since photons undergoing scattering and diffraction have different transfer functions as they travel through muscle, we proposed and successfully demonstrated the use of polarization gating to separate diffracted signal from scattered noise. This improvement enables fast collection of large samples of sarcomere lengths in diseased muscles.

Second and the main goal of this thesis, we proposed in Chapter 3 a new principle for collecting sarcomere length data that is theoretically compatible with the requirements for collecting sarcomere length during movement: real-time sampling, compatibility with gross movement, inducing minimal tissue damage, and resolving nanometer-scale protein geometry change. Towards this goal, we theoretically developed and performed computer

simulations of a new technique termed resonant reflection spectroscopy (RRS). Skeletal muscle sarcomeres provide a unique super-periodic structure that interacts strongly with laser light. In traditional laser diffraction, sarcomeres are illuminated perpendicular to the long axes, and the sarcomere periodicity acts as a volumetric phase grating. The resulting diffraction patter is used to calculate sarcomere length. RRS is minimally invasive because illumination and collection occurs with a single fiber optic probe that is aligned parallel to the sarcomere long axis. The trade-off of this geometry is the need for dramatically increased wavelength range that is not met by typical laser emitters. This challenge, though, has the additional benefit of providing rich structural information about the sarcomere microstructure.

Next, we showed proof of concept for minimally invasive RRS in chapter 4. We used a new super-continuum source that was originally conceptualized for fiber optic communication. In 10 muscles, we show close agreement and significant correlation between sarcomere lengths measured by traditional laser diffraction and the RRS concept. We achieved sub-micrometer resolution, which provided sufficient detail of sarcomere structure.

Building upon our proof of concept, we extended our work and established feasibility for in vivo, real-time, functional sarcomere length by RRS in Chapter 5. Optical frequency domain interferometry, another concept from optical communication technology, enabled profile sarcomere structure across millimeters of tissue, minimally-invasively, during movement and activity. We showed sarcomere lengths during passive strain, twitch and isometric contractions of a muscle tendon unit in the rabbit leg. Importantly, we met the necessary metrics we set out to achieve: real-time sampling,

compatibility with gross movement, inducing minimal tissue damage, and resolving nanometer-scale protein geometry change.

Lastly, we addressed the lack of commercial technology to perform RRS in vivo. We developed design rules and demonstrated a laser system that can be used in future RRS systems. Using an optical parametric oscillator scheme, we determined optimization procedures that proved necessary to increase sweep speeds to RRS relevant levels. By using these procedures, we achieved 422 nm bandwidth operated at 14 kHz sweep rate.

7.2 Future Directions

The true importance of this dissertation is in applying these new methods and principles to study normal and diseased movement. Extensive work can be done in animal models with the knowledge provided in this thesis. However, extension to clinical trials likely requires additional practical developments. First and foremost are improvements to fiber optic probes for RRS. Probes that have enough mechanical strength for patient insertion, particularly to diseased tissue, are required. Fortunately, many surface coatings and metallization techniques exist that can be used towards this goal. Also, more tissue can be sampled at higher SNR with improvements to the geometry of the optical probe. Towards this goal, fiber optic lens systems have been included in smaller than 30 gauge hypodermic needles.

Once a commercial grade system is developed, the potential impact of using RRS methods and principles are staggering. Previously un-obtainable data of protein structure during normal and diseased movement will be accessible. Equally important, RRS will enable monitoring of protein adaptation to pharmacological, physical therapy, and

surgical treatment. Patients with cerebral palsy, Parkinson's disease, muscular dystrophy and stroke stand to benefit from these new research avenues.